Commun Nonlinear Sci Numer Simulat 93 (2021) 105529

Contents lists available at ScienceDirect

Commun Nonlinear Sci Numer Simulat

journal homepage: www.elsevier.com/locate/cnsns

Research paper

Revealing the role of the effector-regulatory t cell loop on autoimmune disease symptoms via nonlinear analysis

Wenjing Zhang[a,*], Pei Yu[b]

[a] Department of Mathematics and Statistics, Texas Tech University, Lubbock, TX, 79409 USA
[b] Applied Mathematics, Western University, London, Ontario, Canada N6A 5B7

ARTICLE INFO

Article history:
Received 30 December 2019
Revised 13 July 2020
Accepted 4 September 2020
Available online 9 September 2020

ABSTRACT

In this paper, we investigate the influence of the effector-regulatory (Teff-Treg) T cell interaction on the T-cell-mediated autoimmune disease dynamics. The simple 3-dimensional Teff-Treg model is derived from the two-step model reduction of an established 5-dimensional model. The reduced 4- and 3-dimensional models preserve the dynamical behaviors in the original 5-dimensional model, which represents the chronic and relapse-remitting autoimmune symptoms. Moreover, we find three co-existing limit cycles in the reduced 3-dimensional model, in which two stable periodic solutions enclose an unstable one. The existence of multiple limit cycles provides a new mechanism to explain varying oscillating amplitudes of lesion grade in multiple sclerosis. The complex multiphase symptom could be caused by a noise-driven Teff population traveling between two coexisting stable periodic solutions. The simulated phase portrait and time history of coexisting limit cycles are given correspondingly.

1. Introduction

1.1. Self-tolerance and T-cell-mediated autoimmune disorder

Self-tolerance is a state in which the immune system can attack foreign pathogens, but avoids mounting tissue-destructive responses against the organism's own body. The failure of self-tolerance mechanisms leads to autoimmunity. However, even for a healthy immune system, both positive and negative selections of T cells during their generation by the thymus, are not fail-proof. This results in the production of auto-reactive T cells to be released to peripheral blood. The escaped auto-reactive T cells are regulated by peripheral tolerance mechanisms to avoid the immune responses against the organism's own tissues. Discrimination of self versus non-self antigens is a delicate process. One common factor in peripheral tolerance, which most studies have focused on, is the interaction between dendritic cells (DCs) and T cells. Great progress has been achieved since the discovery of regulatory T cells by Sakaguchi et al. in 1995 [22].

The DC-T-cell interaction occurs in the adaptive immune response. It is initiated when immature DCs, such as professional antigen presenting cells (pAPCs), settle at a site of infection or inflammation and then become activation and mature. Upon being activated, the pAPCs provide essential signals to transform naive T cells, with the same specific antigen receptor, into effector T cells. The activation process of the naive T cells is combined with a proliferation phase, which seems to require

* Corresponding author.
E-mail addresses: wenjing.zhang@ttu.edu (W. Zhang), pyu@uwo.ca (P. Yu).

https://doi.org/10.1016/j.cnsns.2020.105529
1007-5704/

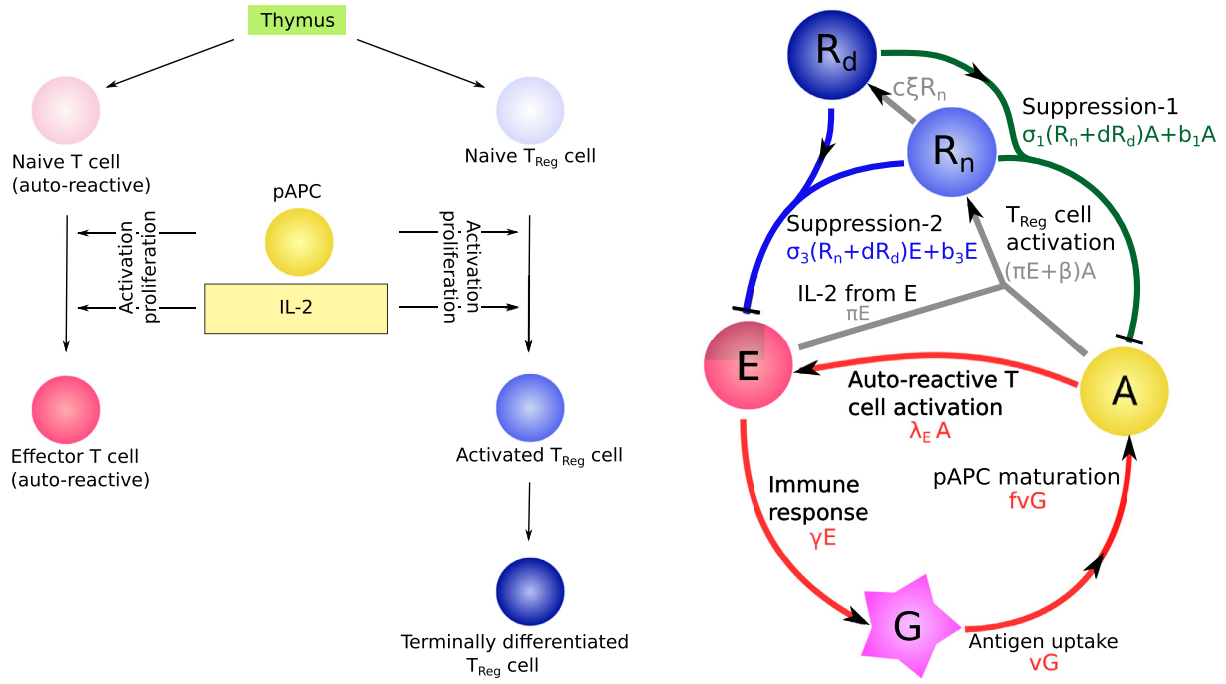

Fig. 1. Diagrams for the DC-T-cell interaction (left panel) and for the mathematical model (1).

cytokine interleukin-2 (IL-2) [7]. Among the naive T cells, there exist auto-reactive T cells which carry specific self-antigen receptors in the periphery and mount a response against the host's own body. The auto-reactive effector T cells (referred as effector T cells in the rest of the text) are regulated by regulatory T cells (T_{Reg}). The T_{Reg} cells show immunosuppressive actions mainly by two mechanisms, one removing pAPCs and another eliminating auto-reactive T cells from the system. A diagram showing the CD-T-cell interaction and corresponding mechanism is given in the left panel of Fig. 1.

The homeostasis between auto-reactive effector T cells and regulatory T cells (Teff-Treg homeostasis) results in a balanced peripheral tolerance state, while a dysfunction or imbalance in the Teff-Treg homeostasis could induce Type 1 diabetes [17], multiple sclerosis [19], and cancer [21]. A broad understanding of the dynamics between the effector T cells and regulatory T cells not only gives new insights in the complex autoimmune symptom, but also promotes therapeutic manipulation.

1.2. The 5-dimensional mathematical model with relapsing-Remitting dynamics

In this paper, the study of T cell-mediated autoimmune disease dynamics is based on an established 5-dimensional ODE model in [32]. The model captures the self-tolerance and autoimmune disorder states, including stable, oscillating, and relapsing-remitting (recurrent) autoimmune disorder solutions. The model is described by the following ODE equations. And the corresponding diagram between various cell population and the mechanisms are provided in the right panel of the Fig. 1.

$$\begin{aligned}
\dot{A} &= f\tilde{\nu}G - \sigma_1(R_n + dR_d)A - b_1A - \mu_A A,\\
\dot{R}_n &= (\pi_3 E + \beta)A - \mu_n R_n - \xi R_n,\\
\dot{R}_d &= c\,\xi R_n - \mu_d R_d,\\
\dot{E} &= \lambda_E A - \sigma_3(R_n + dR_d)E - b_3E - \mu_E E,\\
\dot{G} &= \gamma E - \tilde{\nu}G - \mu_G G,
\end{aligned} \tag{1}$$

where the dot denotes differentiation with respect to time t, and A, R_n, R_d, E and G represent respectively the cell populations of mature pAPCs, active, terminally differentiated T_{Reg}, auto-reactive effector T cells, and the particular self-antigen of interest. All cell populations are specific for a given self-antigen. The cycle of autoimmunity starts at pAPCs (A) up-taking self antigen (G) at the rate of $\tilde{\nu}G$. Upon taking up a given antigen molecule, the probability of the maturation of this pAPC is denoted as f ($0 < f < 1$). The mature pAPCs then activate naive T cells, including both auto-reactive T cells and T_{Reg} cells. The activation and proliferation process requires IL-2 [7], which is produced by the auto-reactive effector T cells themselves at the rate of $\pi_3 EA$, from other sources, such as DCs and/or conventional T cells [10,26], at the rate of β. Recent experiments discovered a new T_{Reg} cells subpopulation, which is generated by conventional natural T_{Reg} cells (nT_{Reg}) [3]. These terminally differentiated suppressors show more efficient suppressible capacity but live with a shorter lifetime. Note that a

Table 1
Parameter values used in previous models [1].

Parameter	Value	Parameter	Value
$\tilde{\nu}$	$0.0025\,A/G$ day	d	2
π_3	$0.0256\,R_n/E/A$/day	c	$2^3 = 8$
λ_E	$1000\,E/A$/day	β	$200\,R_n/A$/day
$\sigma_{1,3}$	$3 \times 10^{-6}/(R_n$ or $R_d)$/day	γ	$2000\,G/E$/day
b_1	0.25/day	b_3	0.25/day
μ_A	0.2/day	μ_E	0.2/day
μ_G	5/day	μ_n	0.1/day
μ_d	0.2/day	ξ	0.025/day
α	A/E/day (Bifur. parameter)	f	$1.0 \times 10^{-4} \in (0,\ 1)$ (Bifur. parameter)
η_1	$b_1 + \mu_A$ (PBP)	η_2	$b_3 + \mu_E$ (PBP)

fraction of T_{Reg} cells, ξR_n, is further developed into terminally differentiated T_{Reg} cells (R_d) at the rate of $c\xi R_n$. After activation, the auto-reactive effector T cells attack the host body and release self-antigen at the rate of γE. This vicious cycle is regulated by the T_{Reg} cells (R_n and R_d) with the particular self-antigen of interest. The down-regulation process removes the auto-reactive effector T cells at the rate of $\sigma_1(R_n + dR_d)A$ and the mature pAPCs at the rate of $\sigma_3(R_n + dR_d)E$. In addition, the T_{Reg} cells carrying other antigens eliminate the mature pAPCs and auto-reactive T cells at rates of b_1A and b_3E. For convenience, the elimination rates of A, R_n, R_d, E, and G are denoted as μ_A, μ_n, μ_d, μ_E, and μ_G, respectively. The definitions of the system parameters can be found in [32], and their values used in model (1) are listed in Table 1, where PBP stands for "Potential Bifurcation Parameter."

1.3. Understanding complex autoimmune symptoms via nonlinear dynamics

The clinical and pathological outcomes of autoimmune diseases are multiple and diverse. Taking multiple sclerosis for example, other than chronic and relapsing-remitting forms of the disease [6], shown in Fig. 2 (a) and (c), we observe that the severity and frequency of autoimmune symptoms vary considerably among individual patients [11]. Experimental data show lesion grade of multiple sclerosis oscillations in high level with multiple amplitudes [4], see Fig. 2(b). This disease outcome pattern can have a dynamical explanation as the coexistence of multiple stable cycles. Complicated dynamical motions travel and shift among coexisting stable cycles in a random manner [2,9]. This idea was first proposed by Earn et al. [9] to explain the irregular dynamics in measles epidemics after the introduction of mass vaccination. Coexisting attractors are revealed in a non-autonomous system by introducing a seasonally varying transmission rate. As to the autonomous systems, the coexisting multiple stable cycles may be generated from Hopf bifurcation. Up to now, most of the established works are limited to bifurcation of the single limit cycle. Two limit cycles can be demonstrated in numerical simulation from a subcritical Hopf bifurcation. But the corresponding analytical study involves large symbolic computation. Identifying multiple limit cycles in disease dynamics could provide new insights in understanding the intrinsic nonlinear interactions. In this paper, we focus on the study of limit cycles arising from Hopf bifurcation. The mathematical theory is related to the well-known Hilbert's 16th problem [13]. Very recently, bifurcation of multiple limit cycles has been found in a 3-dimensional physical system [18], and in 2-dimensional population and disease models [15,29,33], showing the interesting bistable or even tri-stable phenomenon, which involves equilibria and oscillating motions.

Nevertheless, other forms of coexisting attractors have been proposed which may cause complex dynamics, such as the coexisting positive stable equilibria, and the coexisting stable equilibria and stable limit cycle. Driven by stochastic noise, the solutions travel within these stable attractors. Because within the reasonable parameter region, the proposed models

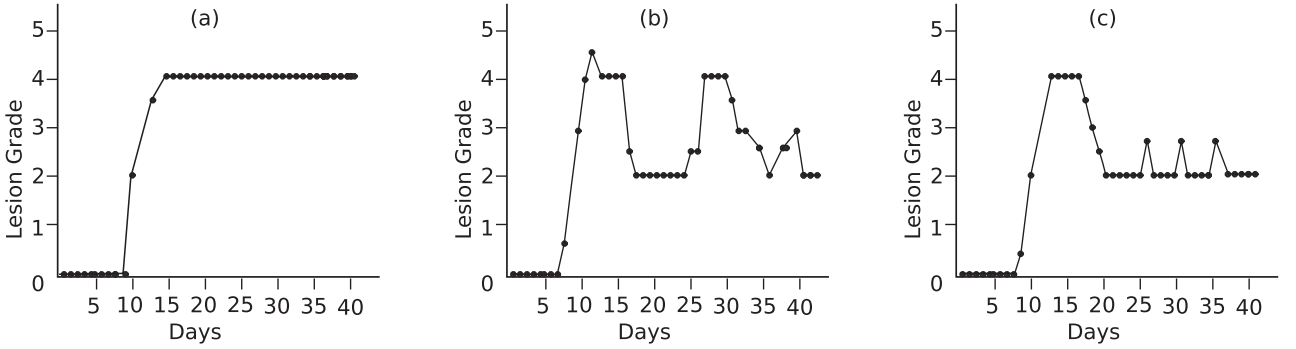

Fig. 2. Clinical courses of multiple sclerosis: (A) Chronic, (B) Multiphase, and (C) Relapse-remitting. Vertical axis denotes the lesion grade. Experimental data is from source [4].

admit one trivial equilibrium solution (boundary equilibrium) and one positive equilibrium solution, and these two equilibrium solutions cannot be simultaneously stable. Thus, the case of coexisting positive stable equilibria does not occur in the models of this paper. Note that no Hopf bifurcation may occur from the trivial equilibrium solution. However, the case of the coexisting positive stable equilibrium and stable limit cycle can be generated by a subcritical Hopf bifurcation on the positive equilibrium. The occurrence of a subcritical Hopf bifurcation induces a stable equilibrium, which is enclosed by a small unstable limit cycle, and further for generalized Hopf bifurcation, a larger stable limit cycle may exist, which encloses the unstable smaller limit cycle and the stable equilibrium. Similarly, if the positive equilibrium is unstable, supercrtical Hopf bifurcation may occur, leading to a stable limit cycle, and further for generalized Hopf bifurcation, there may exist a large usstable limit cycle which enclosed the smaller stable limit cycle and the unstable equilibrium. Such bifurcations may cause complex dynamics in the system. In this paper, we will pay particular attention on the multiple limit cycles due to Hopf bifurcation.

The rest of the paper is organized as follows. To facilitate revealing the dynamics of the Teff-Treg loop, in Section 2, we introduce model reductions via an iterative formula based on geometric singular perturbation theory. Bifurcation analysis results and numerical simulations demonstrate that the two reduced models inherit the intrinsic dynamical behaviors from the original model. The proof of the existence of three limit cycles and the corresponding simulation in non-scaled parameter values are proved in Section 3. Conclusion and discussion are drawn in Section 4.

2. Model reductions and comparison

2.1. Model reduction from 5 dimension to 4 dimension

The first step in model reduction is based on the Geometric Singular Perturbation Theory (GSPT) [23], which eliminates the fast variable by substituting it with its higher-order approximation. The following multiple time scale ODE model illustrates the basic idea,

$$\dot{X} = f(t, X, Y, \epsilon), \qquad \epsilon\dot{Y} = g(t, X, Y, \epsilon), \tag{2}$$

where the slow variable is denoted as $X \in R^m$, the fast variable as $Y \in R^n$, $t \in R$ denotes time, and ϵ is a small perturbation $(0 < \epsilon \ll 1)$. Here, the fast variable $Y(t, \epsilon) = h(t, X, \epsilon)$ is considered as the integral manifold with an asymptotic expansion, given by

$$h(t, X, \epsilon) = \phi(X, t) + \epsilon h_1(X, t) + \epsilon^2 h_2(X, t) + \cdots, \tag{3}$$

where $h(t, X, 0) = \phi(X, t)$, solved from $g(t, X, Y, 0) = 0$, is a zero-order approximation of the slow integral manifold. The approximation of $h(t,X,\epsilon)$ in (3) gets better with the increase of the ϵ terms. Consequently, the solution of the following equation:

$$\dot{X} = f(t, X, h(t, X, \epsilon)), \tag{4}$$

provides a good approximate solution for the original system (2) restricted to the slow manifold. Note that the Quasi-Steady State Assumption (QSSA) [25] can be represented by the similar form of equations:

$$\dot{X} = f(t, X, Y, \epsilon), \qquad 0 = g(t, X, Y, \epsilon). \tag{5}$$

Considering the parameter values in Table 1, we rewrite model (1) as

$$\begin{aligned} \dot{x} &= \zeta(x, \epsilon) + \tilde{F}(x, \epsilon)y, \\ \epsilon\dot{y} &= \xi(x, \epsilon) + \tilde{G}(x, \epsilon)y, \end{aligned} \tag{6}$$

where $\epsilon = 1/\gamma$, with x being the slow variable and y the fast variable, and

$$x = \begin{pmatrix} A \\ R_n \\ R_d \\ E \end{pmatrix}, \quad \zeta(x, \epsilon) = \begin{pmatrix} -\sigma_1(R_n + dR_d)A - b_1A - \mu_A A \\ (\pi_3 E + \beta)A - \mu_n R_n - \xi R_n \\ c\,\xi R_n - \mu_d R_d \\ \lambda_E A - \sigma_3(R_n + dR_d)E - b_3 E - \mu_E E \end{pmatrix}, \tag{7}$$

$$\tilde{F} = (f\tilde{\nu}, 0, 0, 0)^T, \quad y = G, \quad \xi(x, \epsilon) = E, \quad \tilde{G} = -\frac{\tilde{\nu} + \mu_G}{\gamma}.$$

Note that the parameter value of γ is much larger than that of the other two parameters $\tilde{\nu}$ and μ_G (see Table 1), and so $\epsilon = 1\gamma$ may be treated as a small perturbation. For the sake of application, we keep the real parameter values in the 5-dimensional system (1) with no dimensionalization. Then, we apply the higher-order approximation analysis to find the solution of system (6). To achieve this, we use the equation for the slow curve $\phi(x)$ [23], and set $\epsilon = 0$ in the second equation of (6) to obtain

$$0 = \xi(x, 0) + \tilde{G}(x, 0)y = E - \frac{\tilde{\nu} + \mu_G}{\gamma}G.$$

The above equation yields a set of critical points (equilibria on the fast manifold), given by

$$G = \frac{\gamma}{\tilde{\nu} + \mu_G} E.$$

Suppose the asymptotic expansion of the solution on the slow manifold is given by $y = h(x, \epsilon) = \phi(x) + \epsilon h_1(x) + \epsilon^2 h_2(x) + \cdots$, which is substituted into the second equation of (6) to yield

$$\epsilon \dot{y} = \epsilon \frac{dh}{dt}(x, \epsilon) = \epsilon \left(\frac{\partial h}{\partial x} \frac{dx}{dt} + \frac{\partial h}{\partial \epsilon} \frac{d\epsilon}{dt} \right) = \xi + \tilde{G} y = \xi + \tilde{G} h(x, \epsilon) = \xi + \tilde{G} h, \quad \text{where} \quad \frac{d\epsilon}{dt} = 0$$

from which we obtain

$$\epsilon \frac{\partial h}{\partial x} \left(\zeta + \tilde{F} h \right) = \xi + \tilde{G} h. \tag{8}$$

Thus, simply solving h from Eq. (8) we get

$$h = \frac{\xi - \epsilon h_x \zeta}{\epsilon h_x \tilde{F} - \tilde{G}}.$$

Now, applying the iterative process algorithm from [20,23,24] gives

$$\varphi^{(0)} = \phi(x) = -\frac{E}{\tilde{G}} = \frac{\gamma}{\tilde{\nu} + \mu_G} E, \quad \varphi^{(k)} = \frac{\xi - \epsilon \varphi_x^{(k-1)} \zeta}{\epsilon \varphi_x^{(k-1)} \tilde{F} - \tilde{G}}, \quad k = 1, 2, \ldots,$$

where

$$\varphi_x^{(0)} = \left(\frac{\partial \varphi^{(0)}}{\partial A}, \frac{\partial \varphi^{(0)}}{\partial R_n}, \frac{\partial \varphi^{(0)}}{\partial R_d}, \frac{\partial \varphi^{(0)}}{\partial E} \right) = \left(0, 0, 0, \frac{\gamma}{\tilde{\nu} + \mu_G} \right).$$

Therefore, the slow invariant manifold in the zero-order approximation is written as

$$G = h(x) = \phi(x) = \frac{\gamma}{\tilde{\nu} + \mu_G} E, \tag{9}$$

which exactly equals that obtained by applying the QSSA method in (5).

Consequently, the reduced 4-dimensional model derived by either the Geometric Singular Perturbation Theory (GSPT) or the QSSA method is given by

$$\begin{aligned}
\dot{A} &= \alpha E - \sigma_1 (R_n + d R_d) A - b_1 A - \mu_A A, \quad \text{where} \quad \alpha = \frac{f \tilde{\nu} \gamma}{\tilde{\nu} + \mu_G}, \\
\dot{R}_n &= (\pi_3 E + \beta) A - \mu_n R_n - \xi R_n, \\
\dot{R}_d &= c \xi R_n - \mu_d R_d, \\
\dot{E} &= \lambda_E A - \sigma_3 (R_n + d R_d) E - b_3 E - \mu_E E.
\end{aligned} \tag{10}$$

It should be noted that the parameter λ_E in the last equation of (10) is also very large, comparing with other parameters in this equation, and so E can also be treated as a fast variable. Hence, we may treat both G and E as fast variables to reduce the 5-dimensional system (1) to a 3-dimensional system. Since the goal of this paper is to investigate the influence of the effector-regulatory T cell loop on the autoimmune disease dynamics, we will focus on the state variables representing the effector and regulatory T cells (E, R_n, and R_d) to obtain a simple model showing the desired disease behaviors (including self-tolerance and relapse-remitting, multiphase courses, and chronic autoimmune symptoms). Therefore, we will choose the variables A and G to reduce the 5-dimensional system (1) to a 3-dimensional system. This is more challenging compared to simply taking the variable E as a fast variable, showing a non-trivial and more interesting reduction process.

2.2. Model reduction from 4 dimension to 3 dimension

The recurrent behavior observed in the 5-dimensional model is inherited by the reduced 4-dimensional model (10), as shown in Figs. 3 and 4. The simulations shown in Fig. 3 indicate that the ratio between the pAPCs (A) and the auto-reactive effector cells (E) approaches to a constant. This implies that either A or E can be reduced. Since this paper studies the effect of interaction between auto-reactive T cells and T_{Reg} cells on autoimmune diseases, we will further use E to represent A.

First, we point out that the proof of the well-posedness of model (10) provided in [32] guarantees the positiveness and boundedness of its solutions. That is, all solutions $A(t)$, $R_n(t)$, $R_d(t)$ and $E(t)$ for $t > 0$ are positive and bounded. Then, we obtain the load of pAPCs by solving the first equation of system (10) for the variable $A(t)$ as follows:

$$A(t) = e^{-\int_0^t g(s) ds} A(0) + \int_0^t \alpha E(s) \, e^{-\int_s^t g(u) du} ds,$$

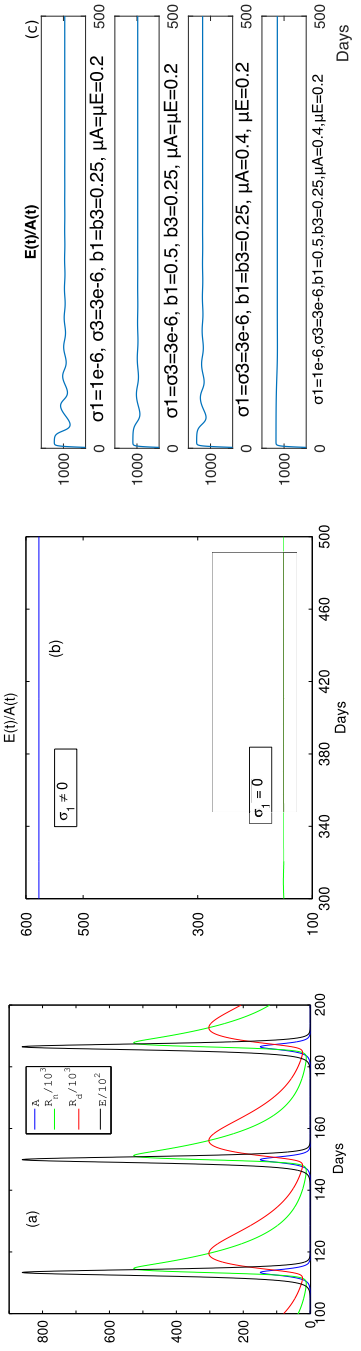

Fig. 3. Time-history of the 4-dimensional model (10).

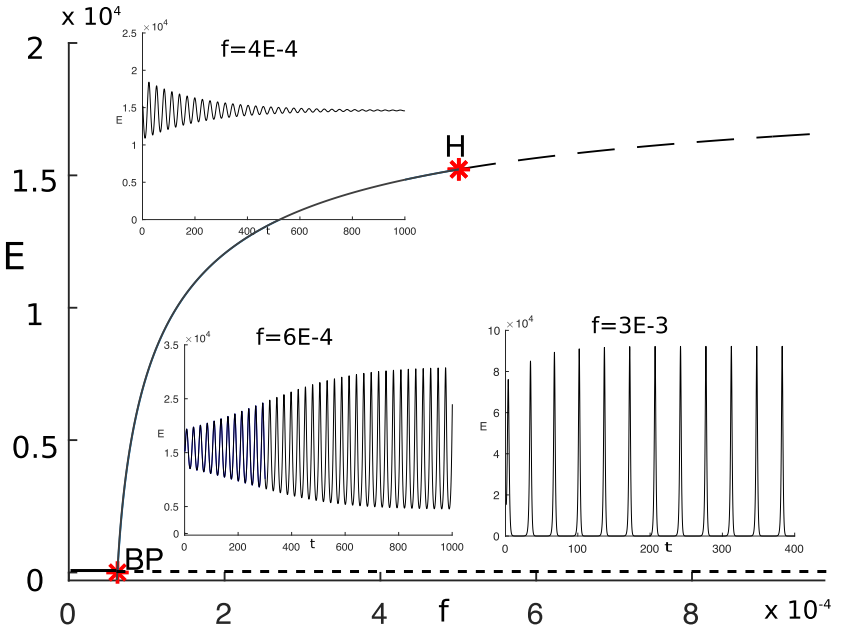

(a) 5-dimensional model (1)

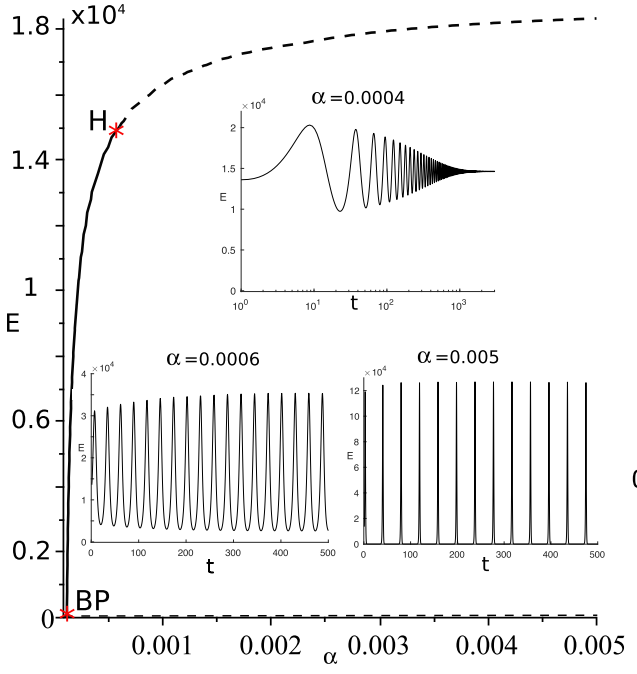

(b) 4-dimensional model (10)

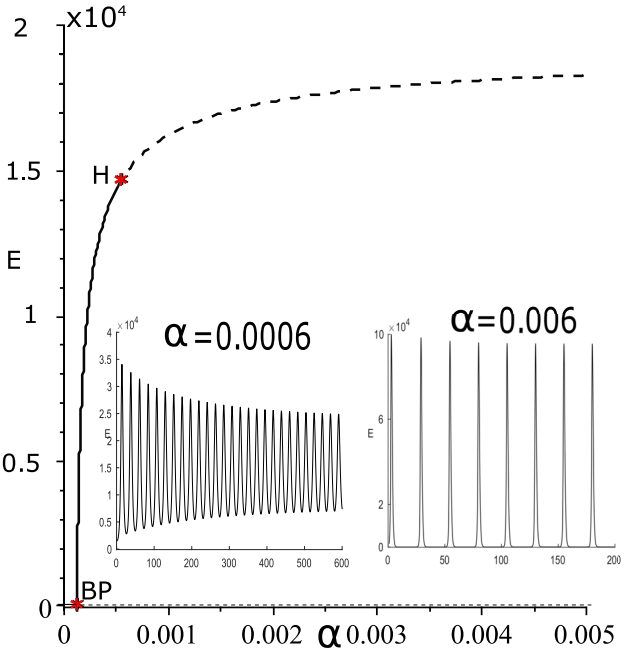

(c) 3-dimensional model (16)

Fig. 4. Bifurcation diagrams of effector T cell E in terms of parameters f and α are plotted in (a) and (b,c). H and BP denote Hopf and transcritical bifurcation critical points.

where

$$g(t) = b_1 + \mu_A + \sigma_1[R_n(t) + dR_d(t)].$$

Let

$$F(t) = A(t) - e^{-\int_0^t g(s)ds}A(0) - \int_0^t \alpha E(s)\, e^{-\int_s^t g(u)du}ds \equiv 0 \quad \text{for} \quad t > 0.$$

Thus,

$$\begin{aligned}0=\lim_{t\to+\infty}F(t)&=\lim_{t\to+\infty}\left[A(t)-e^{-\int_0^t g(s)ds}A(0)-\int_0^t \alpha E(s)\,e^{-\int_s^t g(u)du}ds\right]\\&=\lim_{t\to+\infty}\left[A(t)-\int_0^t \alpha E(s)\,e^{-\int_s^t g(u)du}ds\right]\\&=\lim_{t\to+\infty}\left[A(t)-\lim_{t\to+\infty}e^{-\int_0^t g(u)du}\int_0^t \alpha E(s)\,e^{-\int_s^0 g(u)du}ds\right]\\&=\lim_{t\to+\infty}\left[A(t)-\frac{\int_0^t \alpha E(s)\,e^{\int_0^s g(u)du}ds}{e^{\int_0^t g(u)du}}\right].\end{aligned}$$

Now it is seen from the second term of the above equation that both the functions on the numerator and denominator of this term are well defined, and the term is in the form of $\left[\frac{\pm\infty}{+\infty}\right]$ with respect to t. Moreover, the derivatives of both two functions with respect to t exist when the solutions of the system are convergent. Therefore, we can apply the L'Hospital's Rule to this term to obtain

$$0=\lim_{t\to+\infty}\left[A(t)-\frac{\alpha E(t)\,e^{\int_0^t g(u)du}}{g(t)e^{\int_0^t g(u)du}}\right]=\lim_{t\to+\infty}\left[A(t)-\frac{\alpha E(t)}{b_1+\mu_A+\sigma_1(R_n(t)+dR_d(t))}\right].$$

Hence, we may assume that in the long run,

$$A(t)=\frac{\alpha\,E(t)}{b_1+\mu_A+\sigma_1[R_n(t)+dR_d(t)]},\quad t\to+\infty. \tag{11}$$

The analogous procedure applied on the last equation of the model (10) yields

$$E(t)=\frac{\lambda_E\,A(t)}{b_3+\mu_E+\sigma_3[R_n(t)+dR_d(t)]},\quad t\to+\infty. \tag{12}$$

According to the parameter values in Table 1, we have $b_1=b_3$, $\mu_A=\mu_E$, and $\sigma_1=\sigma_3$. The Eqs. (11) and (12) yield

$$\left[\frac{A(t)}{E(t)}\right]^2=\frac{\alpha}{\lambda_E}\quad\Longrightarrow\quad\frac{A(t)}{E(t)}=\sqrt{\frac{\alpha}{\lambda_E}},\quad t\to+\infty. \tag{13}$$

The preceding equation shows a proportional relation between $E(t)$ and $A(t)$ when the solutions of the system (10) converge.

In a case that the parameter values in system (10) give periodic solutions, a numerical simulation in Fig. 3(b) still demonstrates the proportional relation between $E(t)$ and $A(t)$. We confirm the result from the simulation by rigorous mathematical proof. Due to the positiveness and boundedness of the solutions in model (10) proved in [32], the first and fourth equations of the system (10) yield that

$$\begin{aligned}\frac{d\left(\frac{A}{E}\right)}{dt}&=\frac{\frac{dA}{dt}E-A\frac{dE}{dt}}{E^2}\\&=\frac{1}{E^2}\left[\alpha E^2-\sigma_1(R_n+dR_d)AE-b_1AE-\mu_AAE-\lambda_EA^2+\sigma_3(R_n+dR_d)AE+b_3AE+\mu_EAE\right]\\&=\alpha-\lambda_E\left(\frac{A}{E}\right)^2,\end{aligned} \tag{14}$$

under the conditions $b_1=b_3$, $\mu_A=\mu_E$, and $\sigma_1=\sigma_3$. We then apply the technique of separating variables to (14) to obtain $\frac{1}{\left[\sqrt{\alpha}+\sqrt{\lambda_E}\left(\frac{A}{E}\right)\right]\left[\sqrt{\alpha}-\sqrt{\lambda_E}\left(\frac{A}{E}\right)\right]}d\left(\frac{A}{E}\right)=dt$ and further $\frac{\sqrt{\alpha}+\sqrt{\lambda_E}\left(\frac{A}{E}\right)}{\sqrt{\alpha}-\sqrt{\lambda_E}\left(\frac{A}{E}\right)}=\exp\left(2\sqrt{\frac{\alpha}{\lambda_E}}\,t\right)$. It is easy to see that the right side of the above equation goes to positive infinity as $t\to+\infty$. Since $\frac{A}{E}$ is bounded according to Eq. (14), we have that the solution of the Eq. (14) converges to its equilibrium

$$\lim_{t\to+\infty}\frac{A}{E}(t)=\sqrt{\frac{\alpha}{\lambda_E}}. \tag{15}$$

In the case that the parameters do not satisfy the conditions: $b_1=b_3$, $\mu_A=\mu_E$, and $\sigma_1=\sigma_3$, the proportional relation between $E(t)$ and $A(t)$ is shown numerically through different choices of parameters in Fig. 3(c).

In order to investigate how the effector-regulatory T cell loop affects the autoimmune disease dynamics, we focus on the state variables E, R_n, and R_d. Thus, substituting $A(t)$ given in (11) into the 4-dimensional model (10) yields a reduced 3-dimensional model as follows:

$$\begin{aligned}\dot{R}_n&=\frac{\alpha(\pi_3E+\beta)E}{(b_1+\mu_A)+\sigma_1(R_n+dR_d)}-(\mu_n+\xi)R_n,\\\dot{R}_d&=c\,\xi R_n-\mu_dR_d,\\\dot{E}&=\frac{\alpha\lambda_EE}{(b_1+\mu_A)+\sigma_1(R_n+dR_d)}-\sigma_3(R_n+dR_d)E-(b_3+\mu_E)E.\end{aligned} \tag{16}$$

2.3. Model comparison through bifurcation analysis

This subsection shows that the intrinsic dynamical behaviors in the original 5-dimensional model (1) are preserved in the reduced 4- and 3-dimensional models in (10) and (16). The qualitative behaviors of the three models are summarized in the bifurcation diagrams in Fig. 4. All three models have a trivial equilibrium E_0 indicating immune tolerance and a non-trivial equilibrium E_1 indicating autoimmunity/autoimmune disorder. Two equilibrium solutions cross and exchange their stability at a transcritical bifurcation, denoted as 'BP' (branching point) in the bifurcation diagrams. Hopf bifurcation occurs from the non-trivial equilibrium E_1 in all three models and serves as an oscillating source. With variation of the bifurcation parameters, all three models exhibit immune tolerance state (no auto-reactive effector T cell E), stable minor autoimmune disorder (small amount of E), oscillating autoimmune disorder (oscillating E value with small period), and recurrent autoimmune disorder (oscillating E value with large period). Detailed bifurcation and stability analyses are given in Appendix A. The summarized analytical results are presented by bifurcation diagrams in Fig. 4 with following details.

- For the 5-dimensional model (1) with $b_1+\mu_A = 0.45\ \text{day}^{-1}$ per A, $b_3+\mu_E = 0.45\ \text{day}^{-1}$ per E and the pAPC-maturation rate f as the bifurcation parameter, a transcritical bifurcation occurs at $(A, R_n, R_d, E, G, f) = (0, 0, 0, 0, 0, 0.6253\times 10^{-4})$, and a Hopf bifurcation at

  $$(A, R_n, R_d, E, G, f) = (10.7712, 50822.5071, 50822.5071, 15226.4112, 6087.706811, 5.0067\times 10^{-4}).$$

  The first Lyapunov coefficient (the first focus value) is -3.4244×10^{-3}, which indicates that the Hopf bifurcation is supercritical and gives rise to stable periodic solutions. Three time-history inserted in Fig. 4(a) show mild, oscillating, and recurrent autoimmune disorders.
- For the 4-dimensional model (10) with $b_1+\mu_A = 0.45\ \text{day}^{-1}$ per A, $b_3+\mu_E = 0.45\ \text{day}^{-1}$ per E and the new pAPC-maturation rate α as the bifurcation parameter, a transcritical bifurcation occurs at $(A, R_n, R_d, E, \alpha) = (0, 0, 0, 0, 1.125\times 10^{-4})$, and a Hopf bifurcation at

  $$(A, R_n, R_d, E, \alpha) = (10.1708, 47530.5529, 47530.5529, 15006.1115, 0.0005).$$

  The first Lyapunov coefficient is -4.800984×10^{-5}, so the Hopf bifurcation is supercritical. The 4-dimensional model shows the same qualitative time-history behaviors as that in the 5-dimensional model.
- For the 3-dimensional model (16) with $b_1+\mu_A = 0.45\ \text{day}^{-1}$ per A, $b_3+\mu_E = 0.25\ \text{day}^{-1}$ per E and the pAPC-maturation rate α as the bifurcation parameter, a transcritical bifurcation occurs at $(R_n, R_d, E, \alpha) = (0, 0, 0, 1.125\times 10^{-4})$, and a Hopf bifurcation at

  $$(R_n, R_d, E, \alpha) = (45467.7438, 45467.7438, 14856.5206, 0.000566).$$

  The first Lyapunov coefficient is -5.458792×10^{-5}, so the Hopf bifurcation is also supercritical. The 3-dimensional model shows the similar qualitative time-history behaviors as the 5- and 4-dimensional models. Two saddle-node bifurcations of periodic orbits happen at $\alpha_{p1} = 5.663989\times 10^{-4}$ and $\alpha_{p2} = 5.663994\times 10^{-4}$, where two limit cycles are generated. This implies the existence of three limit cycles where $\alpha\in(\alpha_{p1}, \alpha_{p2})$. We prove this prediction in the next section. Note that since α is a combination of the parameters $\tilde{\nu}$, μ_G, f and γ, the actural region in the original parameter space is not small.

The bifurcation diagrams and analysis results are obtained by using the numerical bifurcation package MatCont [8]. The other parameter values are taken from Table 1. Both the iterative method and the QSSA method are an approximation of the slow invariant manifold. Therefore, the desired model behaviors is changed during model reduction procedures. With properly chosen parameter values, the three models demonstrate the same qualitative dynamical behaviors, which confirms that the reduced models (10) and (16) are reliable and requires less computation in analysis.

3. Bifurcation of multiple limit cycles in the 3-dimensional model

The diverse oscillating amplitudes of the lesion grades in multiple sclerosis indicates that the Teff-Treg interaction might have coexisting stable periodic solutions. To investigate this hypothesis, we focus on the 3-dimensional Teff-Treg model and study the coexisting multiple periodic solutions. We first briefly explain how to use the method of normal forms to study bifurcation of multiple limit cycles. Suppose the general nonlinear differential system under consideration is given in the form of

$$\dot{\mathbf{z}} = J(\tilde{\zeta})\mathbf{z} + \mathbf{f}(\mathbf{z}, \tilde{\zeta}), \quad \mathbf{z}\in R^n, \quad \tilde{\zeta}\in R, \tag{17}$$

where $\tilde{\zeta}$ is a parameter, $J(\tilde{\zeta})\mathbf{z}$ and $\mathbf{f}(\mathbf{z}, \tilde{\zeta})$ represent the linear and nonlinear parts of the system, respectively. We assume $\mathbf{f}$ is analytic and $\mathbf{f}(\mathbf{0}, \tilde{\zeta}) = \mathbf{0}$, implying that $\mathbf{z} = \mathbf{0}$ is an equilibrium point of the system for all μ. (If the equilibrium is not at the origin, one can simply use a translation to shift it to the origin.) So $J(\tilde{\zeta})$ is the Jacobian of the system evaluated at the equilibrium point $\mathbf{z} = \mathbf{0}$. Further, suppose that at a critical point $\tilde{\zeta} = \tilde{\zeta}_c$, J contains a purely imaginary pair and its other eigenvalues have negative real part. Then by applying a linear transformation $\mathbf{z} = T\mathbf{x}$ and a shifting on the parameter, $\tilde{\zeta} = \tilde{\zeta}_c + \zeta$, we obtain a new system,

$$\dot{\mathbf{x}} = \Lambda(\zeta)\mathbf{x} + F(\mathbf{x}, \zeta), \tag{18}$$

whose Jacobian matrix $\Lambda(\zeta)$ is now in the Jordan canonical form, with

$$\Lambda(\zeta)=\begin{bmatrix}\Lambda_1(\zeta) & 0\\ 0 & \Lambda_2(\zeta)\end{bmatrix},\qquad \text{where}\quad \Lambda_1(\zeta)=\begin{bmatrix}\alpha(\zeta) & \omega(\zeta)\\ -\omega(\zeta) & \alpha(\zeta)\end{bmatrix},$$

and $\Lambda_2(\zeta)$ is an $(n-2)\times(n-2)$ matrix, corresponding to the remaining $n-2$ eigenvalues with negative real part. Note that $\alpha(0)=0$ and $\omega(0)=\omega_c>0$, and that the transversality condition is given by

$$v_0=\left.\frac{d\alpha(\zeta)}{d\zeta}\right|_{\zeta=0}\neq 0.$$

Next, with center manifold theory [5] and normal form theory of Hopf bifurcation [12,13], we apply the following nonlinear transformations:

$$x_1=\omega_c v+\sum_{i+j=k} a_{ij}u_1^i u_2^j,\quad x_2=-\omega_c u+\sum_{i+j=k} b_{ij}u_1^i u_2^j,\quad x_3=\cdots,\quad \cdots,\quad x_n=\cdots,$$

where x_1 and x_2 correspond to the normal form transformation while x_3, $\cdots$, x_n correspond to the center manifold transformation into system (18) to obtain the normal form,

$$\begin{aligned}\dot{u}_1&=v_0u_1+\tau_0u_2+v_1u_1(u_1^2+u_2^2)-\tau_1u_2(u_1^2+u_2^2)+v_2u_1(u_1^2+u_2^2)^2-\tau_2u_2(u_1^2+u_2^2)^2+\cdots\\ \dot{u}_2&=v_0u_2-\tau_0u_1+v_1u_2(u_1^2+u_2^2)-\tau_1u_1(u_1^2+u_2^2)+v_2u_2(u_1^2+u_2^2)^2-\tau_2u_1(u_1^2+u_2^2)^2+\cdots.\end{aligned}$$

Finally, applying the polar coordinate transformation: $u_1=r\sin\theta,\ u_2=r\cos\theta$ into the above equations yields the following normal form in the polar coordinates up to the $(2k+1)$th order term:

$$\begin{aligned}\dot{r}&=r\,(v_0\zeta+v_1r^2+v_2r^4+\cdots+v_kr^{2k}),\\ \dot{\theta}&=\omega_c+\tau_0\zeta+\tau_1r^2+\tau_2r^4+\cdots+\tau_kr^{2k},\end{aligned}\tag{19}$$

where τ_0 is also obtained from the linear analysis, r and θ denote the amplitude and phase of motion, respectively. Both v_k and τ_k are explicitly expressed in terms of the original system's coefficients. v_k is called the kth-order Lyapunov constant (or kth-order focus value) of the Hopf-type critical point (the origin). v_k and τ_k ($k\geq 1$) are obtained by using some symbolic computation software package.

The basic idea of finding k small-amplitude limit cycles of the dynamical system, $\dot{\mathbf{z}}=J(\tilde{\zeta})\mathbf{z}+\mathbf{f}(\mathbf{z},\tilde{\zeta})$ around the origin is as follows: first, find the conditions such that $v_0=v_1=\cdots=v_{k-1}=0$ (note that $v_0=0$ is automatically satisfied at the critical point), but $v_k\neq 0$, and then perform appropriate small perturbations to show the existence of k limit cycles.

We should point out that the linear transformation used to get the system (18) can be very involved, in particular for systems with dimension higher than three. Moreover, in general, even the original system (17) has a simple form, the transformed system (18) may be much more complicated. However, this process is not avoidable in order to calculate the focus values for the Hopf bifurcation analysis and determining the limit cycles and their stability.

3.1. Three limit cycles arising from hopf bifurcation

In this subsection, we will use the 3-dimensional model (16) to prove the existence of three limit cycles bifurcating from a degenerate Hopf critical point. To simplify the analysis, we let $\sigma_1=0$ in (16), which yields

$$\begin{aligned}\dot{R}_n&=\frac{\alpha(\pi_3E+\beta)E}{(b_1+\mu_A)}-(\mu_n+\xi)R_n,\\ \dot{R}_d&=c\,\xi R_n-\mu_dR_d,\\ \dot{E}&=\frac{\alpha\lambda_EE}{(b_1+\mu_A)}-\sigma_3(R_n+dR_d)E-(b_3+\mu_E)E.\end{aligned}\tag{20}$$

To further simplify the analysis, introducing the following dimensionless variables:

$$R_n=\mu_1X,\quad R_d=\mu_2,Y,\quad E=\mu_3Z,\quad \tau=\mu_4t,\tag{21}$$

where $\mu_1=\frac{(b_3+\mu_E)^2}{c\xi\sigma_3d}$, $\mu_2=\frac{b_3+\mu_E}{\sigma_3d}$, $\mu_3=\frac{(b_1+\mu_A)(b_3+\mu_E)^3}{\alpha\beta c\xi\sigma_3d}$, $\mu_4=b_3+\mu_E$, into (20) we obtain

$$\begin{aligned}\frac{dX}{d\tau}&=m_1Z^2+Z-m_2X,\\ \frac{dY}{d\tau}&=X-m_3Y,\\ \frac{dZ}{d\tau}&=m_4Z-m_5XZ-YZ-Z,\end{aligned}\tag{22}$$

where $m_1 = \frac{\pi_3(b_1+\mu_A)(b_3+\mu_E)^3}{\alpha\beta^2 c\xi\,\sigma_3\,d}$, $m_2 = \frac{\mu_n+\xi}{b_3+\mu_E}$, $m_3 = \frac{\mu_d}{b_3+\mu_E}$, $m_4 = \frac{\alpha\,\lambda_E}{(b_1+\mu_A)(b_3+\mu_E)}$, $m_5 = \frac{b_3+\mu_E}{c\xi\,d}$. The parametrization using μ_k, $k = 1,2,3,4$ makes the new variables, X, Y, Z, and the new parameters, m_k, $k = 1, 2, \cdots, 5$ dimensionless. For example, μ_3 has the unit $[E]$, yielding Z dimensionless.

Using the parameter values given in Table 1 and assuming $\alpha = 0.0005$, we have $\mu_1 = 168,750\,[R_n]$, $\mu_2 = 75,000\,[R_d]$, $\mu_3 = 1708597.75\,[E]$, $\mu_4 = 0.45/$ day, which agree with the units of the state variables and time. Moreover, the new parameters are indeed dimensionless, given by

$$m_1 = \frac{2187}{50} = 43.74, \quad m_2 = \frac{5}{18} \approx 0.277778, \quad m_3 = \frac{4}{9} \approx 0.444444,$$
$$m_4 = \frac{200}{81} \approx 2.469136, \quad m_5 = \frac{9}{8} = 1.125. \tag{23}$$

It is easy to obtain two equilibrium solutions from (22) as follows:

$$\mathrm{E}_0 : (0,0,0), \quad \mathrm{E}_1 : \left(\frac{m_3(m_4-1)}{1+m_3m_5}, \frac{(m_4-1)}{1+m_3m_5}, \frac{1}{2m_1}\left(\sqrt{1+\tfrac{4m_1m_2m_3(m_4-1)}{1+m_3m_5}}-1\right)\right), \quad (m_4 \geq 1). \tag{24}$$

A simple linear analysis based on the Jacobian of (22) shows that when $m_4 < 1$, the immune-tolerance equilibrium E_0 is stable while the autoimmune-disorder equilibrium E_1 does not exist; when $m_4 > 1$, E_0 becomes unstable and E_1 emerges to exist. The characteristic polynomial for E_1 is given by $P_1(\lambda) = \lambda^3 + a_1\lambda^2 + a_2\lambda + a_3$, where $a_1 = m_2 + m_3$, $a_2 = m_2m_3 + \frac{m_5a_3}{1+m_3m_5}$, and

$$a_3 = \frac{1}{2m_1}\sqrt{1+m_3m_5+4m_1m_2m_3(m_4-1)}\left(\sqrt{1+m_3m_5+4m_1m_2m_3(m_4-1)}-\sqrt{1+m_3m_5}\right).$$

It is obvious that $a_3 > 0$ when $m_4 > 1$, and $a_3 = 0$ when $m_4 = 1$, indicating that $m_4 = 1$ is a transcritical point between the two equilibrium solutions E_0 and E_1. Note that $a_1 > 0$ for any positive values of the parameters, and a_2, $a_3 > 0$ for $m_4 \geq 1$. Therefore, when $m_4 > 1$, the only possible bifurcation which may occur from the autoimmune-disorder equilibrium E_1 is Hopf bifurcation. The Hopf critical point is determined by the condition, $\Delta_2 = a_1a_2 - a_3 = 0$, where

$$\Delta_2 = \frac{1}{2m_1(1+m_3m_5)}\Big[2m_1m_2m_3m_5(m_2+m_3)(1+m_3m_5) - (1-m_2m_5)\sqrt{1+m_3m_5+4m_1m_2m_3(m_4-1)}$$
$$\times\left(\sqrt{1+m_3m_5+4m_1m_2m_3(m_4-1)}-\sqrt{1+m_3m_5}\right)\Big].$$

It is seen that when $m_4 > 1$, $\Delta_2 > 0$ if $m_2m_5 \geq 1$. In other words, the autoimmune-disorder equilibrium E_1 exists when $m_4 > 1$ and always stable if $m_2m_5 \geq 1$.

Now suppose $m_4 > 1$ and $m_2m_5 < 1$. Then, we may determine one parameter from the equation $\Delta_2 = 0$ to get the Hopf critical condition. Since both m_1 and m_4 contain the parameter α, if we choose α as the bifurcation parameter, we may use both m_1 and m_4 to determine the Hopf critical point, so that the computation becomes simpler. Thus, let

$$m_4 = 1 + \frac{15(1+m_3m_5)}{4m_1m_2m_3}. \tag{25}$$

Then, we have $\mathrm{E}_1 : \left(\frac{15m_3}{4m_1m_2m_3}, \frac{15}{4m_1m_2m_3}, \frac{3}{2m_1}\right)$. It follows that $\Delta_2 = \frac{1}{m_1}\left[m_1(m_2+m_3)m_2m_3 - 6(1-m_2m_5)\right]$. Solving $\Delta = 0$ for m_1 we find the Hopf critical point, defined by

$$m_{1\mathrm{H}} = \frac{6(1-m_2m_5)}{m_2m_3(m_2+m_3)}, \quad (m_2m_5 < 1), \tag{26}$$

where the subscript H denotes Hopf bifurcation. Further, suppose the characteristic polynomial equation $P_1(\lambda) = 0$ has one real eigenvalue $\lambda_1(m_1)$ and a pair of complex conjugate, $\lambda_{2,3}(m_1) = \alpha(m_1) \pm i\,\omega(m_1)$. It should be noted that $\lambda(m_1)$, $\alpha(m_1)$ and $\omega(m_1)$ contain other parameters, m_2, m_3 and m_5. Then, at this critical point $m_1 = m_{1\mathrm{H}}$, we have $\lambda_1(m_{1\mathrm{H}}) = -(m_2 + m_3) < 0$, $\alpha(m_{1\mathrm{H}}) = 0$, and $\omega(m_{1\mathrm{H}}) = \omega_c = \sqrt{\frac{m_2m_3(1+m_3m_5)}{1-m_2m_5}} > 0$. Moreover, we can show that the transversal condition is satisfied:

$$\frac{\partial\,\alpha}{\partial\,m_1}(m_{1\mathrm{H}}) = \frac{-m_2^2m_3^2(m_2+m_3)^2}{12[\,m_2(m_2+2m_3)(1-m_2m_5)+m_3(m_2+m_3)\,]} < 0.$$

Next, introducing the following affine transformation,

$$\begin{pmatrix} X \\ Y \\ Z \end{pmatrix} = \begin{pmatrix} \frac{15m_3}{4m_1m_2m_3} \\ \frac{15}{4m_1m_2m_3} \\ \frac{3}{2m_1} \end{pmatrix} + T\begin{pmatrix} x_1 \\ x_2 \\ x_3 \end{pmatrix}, \tag{27}$$

where

$$T=\begin{bmatrix} 4T_c & -\frac{4\omega_c}{m_2}T_c & -\frac{4}{m_3} \\ -4m_5T_c & -\frac{4(1-m_2m_5)\omega_c}{m_2m_3}T_c & \frac{4}{m_2m_3} \\ 1 & 0 & 1 \end{bmatrix},$$

in which $T_c=\frac{(1-m_2m_5)}{(m_2+m_3)[1+(m_3-m_2)m_5]}$, into system (22) we obtain

$$\begin{aligned}
\frac{dx_1}{d\tau} &= \omega_c x_2+\tfrac{1}{2C_1}\Big[3(1-m_2m_5)^2x_1^2-C_2x_3^2-2C_4x_1x_3+8C_3(x_1+x_3)x_2\Big],\\
\frac{dx_2}{d\tau} &= -\omega_c x_1-\tfrac{1}{2C_1}\Big[3C_3x_1^2+C_5x_3^2+2C_6x_1x_3-8(1-m_2m_5)^2(x_1+x_3)x_2\Big],\\
\frac{dx_3}{d\tau} &= -(m_2+m_3)x_3-\tfrac{(1-m_2m_5)^2}{2C_1}\Big[3x_1^2+11x_3^2+14x_1x_3-\tfrac{8\omega_c}{m_2+m_3}(x_1+x_3)x_2\Big],
\end{aligned}\tag{28}$$

where

$$\begin{aligned}
C_0 &= \frac{1-m_2m_5}{m_2m_3},\\
C_1 &= m_2(m_2+2m_3)(1-m_2m_5)+m_3(m_2+m_3),\\
C_2 &= C_0\Big[m_2(8m_2+5m_3)(1-m_2m_5)+8m_3(m_2+m_3)\Big],\\
C_3 &= C_0\Big[m_2(1-m_2m_5)+m_3\Big]\omega_c,\\
C_4 &= C_0\Big[m_2(4m_2+m_3)(1-m_2m_5)+4m_3(m_2+m_3)\Big],\\
C_5 &= \frac{C_0}{1+m_3m_5}\Big\{(1-m_2m_5)\Big[11m_2+8m_3-m_2m_5(8m_2+5m_3)\Big]+3m_3(1+m_3m_5)\Big\}\omega_c,\\
C_6 &= \frac{C_0}{1+m_3m_5}\Big\{(1-m_2m_5)\Big[7m_2+4m_3-m_2m_5(4m_2+m_3)\Big]+3m_3(1+m_3m_5)\Big\}\omega_c.
\end{aligned}\tag{29}$$

To analyze the co-existing multiple limit cycle, we need the following theorem.

Theorem 3.1 [13]. *Suppose that the focus values of a dynamical system depend on k parameters, expressed as $v_j=v_j(\epsilon_1,\epsilon_2,\ldots,\epsilon_k)$, $j=0,1,\ldots,k$, satisfying $v_j(0,\cdots,0)=0$, $j=0,1,\ldots,k-1$, $v_k(0,\cdots,0)\neq 0$, and $\det\Big[\frac{\partial(v_0,v_1,\ldots,v_{k-1})}{\partial(\epsilon_1,\epsilon_2,\ldots,\epsilon_k)}(0,\cdots,0)\Big]\neq 0$. Then, for any given $\epsilon_0>0$, there exist $\epsilon_1,\epsilon_2,\ldots,\epsilon_k$, and $\delta>0$ with $|\epsilon_j|<\epsilon_0$, $j=1,2,\ldots,k$, such that the equation $\dot r=0$ has exactly k real positive roots for r (i.e., the system has exactly k limit cycles) in a δ-ball with the center at the origin.*

Now we apply the Maple program, developed by [1–9,11–33] for computing the normal forms of Hopf and generalized Hopf bifurcation, to system (28) to obtain the first-order focus value:

$$\begin{aligned}
v_1 = \frac{(1-m_2m5)^2C_0}{(m_2+m3)C_1(C_1+3m_2m_3(1+m_3m_5)\omega_c}\Big[& m_2^3(m_2-m_3)(3m_2-m_3)(4m_2+5m_3)\,m_5^2\\
&-2m_2(12m_2^4-6m_2^3m_3-24m_2^2m_3^2+19m_2m_3^3+17m_3^4)m_5\\
&+12m_2^4-11m_2^3m_3-54m_2^2m_3^2-11m_2m_3^3+12m_3^4\Big],
\end{aligned}$$

where C_0 and C_1 are given in (29), and the lengthy expressions of v_2 and v_3 are given in Appendix B. Eliminating m_5 from the equations $v_1=v_2=v_3=0$ yields two resultants R_1 and R_2, given below.

$$\begin{aligned}
R_1 = m_3(m_2+m_3)(&382993712640m_2^{14}-2468813499792m_2^{13}m_3-2,505,129,112,368m_2^{12}m_3^2\\
&+19404049804717m_2^{11}m_3^3+5219812803460m_2^{10}m_3^4-56169587613643m_2^9m_3^5-4550405074296m_2^8m_3^6\\
&+80872559181716m_2^7m_3^7-4,550,405,074,296m_2^6m_3^8-56169587613643m_2^5m_3^9+5219812803460m_2^4m_3^{10}\\
&+19404049804717m_2^3m_3^{11}-2505129112368m_2^2m_3^{12}-2468813499792m_2m_3^{13}+382993712640m_3^{14}),
\end{aligned}$$

$$\begin{aligned}
R_2 = m_3(m_2+m_3)(&11550682788957468502917120 0m_2^{28}+450222689604990045276979200m_2^{27}m_3\\
&-37875283963356971237606682624m_2^{26}m_3^2+13974551364129617677466651 5008m_2^25m_3^3\\
&+284,816,537,546,699,598,961,284,939,088m_2^{24}m_3^4-17235928505066897788307510307 56m_2^{23}m_3^5\\
&-36702690113194965478013735700 5m_2^{22}m_3^6+97890052769204351241800509486 98m_2^{21}m_3^7\\
&-59642234000658757818646641222 57m_2^{20}m_3^8-28984737061956193514958093718206m_2^{19}m_3^9\\
&+35,371,467,678,053,842,190,106,965,542,250m_2^{18}m_3^{10}+40947994302655830081652722612998m_2^{17}m_3^{11}
\end{aligned}$$

$$
\begin{aligned}
&- 827132104594665918782215266887 83m_2^{16}m_3^{12} - 208879237650409715402965499839 98m_2^{15}m_3^{13}\\
&+ 108289991024276586687163544516454m_2^{14}m_3^{14} - 208879237650409715402965499839 98m_2^{13}m_3^{15}\\
&- 827132104594665918782215266887 83m_2^{12}m_3^{16} + 409479943026558300816527226129 98m_2^{11}m_3^{17}\\
&+ 353714676780538421901069655422 50m_2^{10}m_3^{18} - 289847370619561935149580937182 06m_2^{9}m_3^{19}\\
&- 596422340006587578186466412225 7m_2^{8}m_3^{20} + 978900527692043512418005094869 8m_2^{7}m_3^{21}\\
&- 367026901131949654780137357005m_2^{6}m_3^{22} - 172359285050668977883075103075 6m_2^{5}m_3^{23}\\
&+ 284816537546699598961284939088m_2^{4}m_3^{24} + 139,745,513,641,296,176,774,666,515,008m_2^{3}m_3^{25}\\
&- 378752839633569712376066826 24m_2^{2}m_3^{26} + 450222689604990045276979200m_2m_3^{27}\\
&+ 115506827889574685029171200m_3^{28})
\end{aligned}
$$

It is seen that both R_1 and R_2 are homogeneous polynomials in m_2 and m_3, implying that there is only one independent parameter in the two resultant equations, and thus in general the two equations cannot have common roots. In fact, we have solved $R_1 = 0$ to find all real solutions, but none of them satisfies $R_2 = 0$. Hence, there do not exist solutions for $\nu_1 = \nu_2 = \nu_3 = 0$ and so four limit cycles are not possible. The next best possibility is to have $\nu_1 = \nu_2 = 0$, but $\nu_3 \neq 0$, resulting in three limit cycles. To achieve this, eliminating m_5 from the two equations: $\nu_1 = \nu_2 = 0$, we obtain a solution $m_5 = \frac{m_{5n}(m_2,m_3)}{m_{5d}(m_2,m_3)}$, where

$$
\begin{aligned}
m_{5n} = \;& 21374144064000m_2^{27} + 118834698528000m_2^{26}m_3 - 479475144148000m_2^{25}m_3^2\\
&- 54812710088152 80m_2^{24}m_3^3 - 135073522496172 16m_2^{23}m_3^4 + 124128084319815 56m_2^{22}m_3^5\\
&+ 117135532565906326m_2^{21}m_3^6 + 148045354846367345m_2^{20}m_3^7 - 262017055499069879m_2^{19}m_3^8\\
&- 862612003920767900m_2^{18}m_3^9 - 260317794638374263m_2^{17}m_3^{10} + 183581450581842059 6m_2^{16}m_3^{11}\\
&+ 2,267,385,996,444,092,787m_2^{15}m_3^{12} - 135779094858370870 4m_2^{14}m_3^{13} - 452916846939250489 1m_2^{13}m_3^{14}\\
&- 138283440910132640 2m_2^{12}m_3^{15} + 4,266,811,161,155,274,661m_2^{11}m_3^{16} + 386775145414481868 8m_2^{10}m_3^{17}\\
&- 146063179312653870 1m_2^{9}m_3^{18} - 346489816199515114 8m_2^{8}m_3^{19} - 724354171263863719m_2^{7}m_3^{20}\\
&+ 139691433787112372 4m_2^{6}m_3^{21} + 826,669,182,455,270,361m_2^{5}m_3^{22} - 150574078703701575m_2^{4}m_3^{23}\\
&- 241722794839289274m_2^{3}m_3^{24} - 368534041992648 36m_2^{2}m_3^{25} + 19698628056951024m_2m_3^{26}\\
&+ 5,508,921,575,646,720m_3^{27},
\end{aligned}
$$

$$
\begin{aligned}
m_{5d} = \;& 21374144064000m_2^{28} + 97,460,554,464,000m_2^{27}m_3 - 595,166,586,196,000m_2^{26}m_3^2\\
&- 4,997,728,501,003,280m_2^{25}m_3^3 - 8150127640756896m_2^{24}m_3^4 + 2550275093933366 0m_2^{23}m_3^5\\
&+ 105,709,969,969,241,342m_2^{22}m_3^6 + 37,475,172,724,792,547m_2^{21}m_3^7 - 406356618265396581m_2^{20}m_3^8\\
&- 634,820,010,442,872,584m_2^{19}m_3^9 + 539323353137185649m_2^{18}m_3^{10} + 2,157,010,906,102,053,040m_2^{17}m_3^{11}\\
&+ 699,469,759,264,830,719m_2^{16}m_3^{12} - 354041964432635719 2m_2^{15}m_3^{13} - 3,718,026,974,248,364,927m_2^{14}m_3^{14}\\
&+ 255570938501957984 2m_2^{13}m_3^{15} + 614875870339030682 5m_2^{12}m_3^{16} + 778637145396485244m_2^{11}m_3^{17}\\
&- 5,230,930,094,879,874,037m_2^{10}m_3^{18} - 319290896282253497 6m_2^{9}m_3^{19} + 2,028,470,002,232,920,821m_2^{8}m_3^{20}\\
&+ 2,674,364,728,431,707,460m_2^{7}m_3^{21} + 136,701,839,232,882,045m_2^{6}m_3^{22} - 962075072633232645m_2^{5}m_3^{23}\\
&- 384974198754672312m_2^{4}m_3^{24} + 8699150645724862 8m_2^{3}m_3^{25} + 86755455828494568m_2^{2}m_3^{26}\\
&+ 15,608,611,130,999,040m_2m_3^{27}),
\end{aligned}
$$

and a resultant, given by

$$
\begin{aligned}
R_{12} = \;& m_3(m_2+m_3)\big[382,993,712,640m_2^{14} - 2,468,813,499,792m_2^{13}m_3 - 2,505,129,112,368m_2^{12}m_3^2\\
&+ 19404049804717m_2^{11}m_3^3 + 5,219,812,803,460m_2^{10}m_3^4 - 56169587613643m_2^{9}m_3^5\\
&- 4,550,405,074,296m_2^{8}m_3^6 + 80872559181716m_2^{7}m_3^7 - 4550405074296m_2^{6}m_3^8\\
&- 56169587613643m_2^{5}m_3^9 + 5,219,812,803,460m_2^{4}m_3^{10} + 19404049804717m_2^{3}m_3^{11}\\
&- 2505129112368m_2^{2}m_3^{12} - 2468813499792m_2m_3^{13} + 382993712640m_3^{14}\big].
\end{aligned}
$$

Numerically solving $R_{12} = 0$ for m_3 satisfying $m_2 > 0$ and $m_3 > 0$, we obtain six solutions:

$$
\begin{aligned}
m_3 = \;& 0.16053345\cdots m_2,\ 0.57628811\cdots m_2,\ 0.62806610\cdots m_2,\\
& 1.59218910\cdots m_2,\ 1.73524315\cdots m_2,\ 6.22923122\cdots m_2,
\end{aligned}
$$

but only the first and last ones satisfy $m_5 > 0$ and $m_2m_5 < 1$. Thus, we have two solutions:

$$
(m_3, m_5) = (0.16053345\cdots m_2,\ 0.64692261\cdots/m_2),\quad (6.22923122\cdots m_2,\ 0.22728360\cdots/m_2),
$$

with $m_2 > 0$ being free to choose.

Considering the reference values given in (23), we choose $m_2 = 0.15$ and taking the second set of solution for m_3 and m_5, we obtain the following set of solution:

$$m_2 = 0.15,\ m_3 \approx 0.93438468,\quad m_5 \approx 1.51522401,\quad m_1 \approx 30.50500042,\quad m_4 \approx 3.11887150, \tag{30}$$

for which $v_0 = v_1 = v_2 = 0$, $v_3 \approx -100322.171764 < 0$. Moreover, at the above critical values, we have $\frac{\partial(v_1,v_2)}{\partial(m_3,m_5)} \approx -3694.965085 \neq 0$. Thus, by Theorem 3.2 we can conclude that system (20) can have three small-amplitude limit cycles near the equilibrium solution E_1 due to Hopf bifurcation. Summarizing the above results we have the following theorem.

Theorem 3.2. *When $m_4 = 1 + \frac{15(1+m_3m_5)}{4m_1m_2m_3}$, system (20) has a Hopf critical point at $m_1 = m_{1H} = \frac{6(1-m_2m_5)}{m_2m_3(m_2+m_3)}$ ($m_2m_5 < 1$). At the critical values, $(m_1, m_3, m_5) = (0.102954\cdots/m_2^3,\ 6.22923\cdots m_2,\ 0.227283\cdots/m_2)$, the focus values at the Hopf critical point satisfy $v_0 = v_1 = v_2 = 0$, but $v_3 < 0$. Thus, perturbing the parameters m_1, m_3 and m_5 around the critical values yields three small-amplitude limit cycles around the origin.*

Although Theorem 3.2 indicates that we may have proper parameter values under which three small-amplitude limit cycles exist, to choose appropriate perturbations on the parameters m_1, m_3 and m_5 such that $0 < v_0 \ll -v_1 \ll v_2 \ll -v_3$ is not easy, in particular, when m_3 and m_5 are solved from a coupled pair of polynomial equations. To achieve this, we first obtain the perturbations on m_3 and m_5 as $m_3 = 0.9343846824 + \varepsilon_1 = 0.6343846824$, $m_5 = 1.5152240140 + \varepsilon_2 = 1.1652240140$, where $\varepsilon_1 = -0.3$, $\varepsilon_2 = -0.35$ for which m_1 and m_4 become $m_1 = 66.3355063219$, $m_4 = 2.0332153874$, and the focus values v_i, $i = 1, 2, 3$ then become $v_1 = -1.92038159$, $v_2 = 0.16939725 \times 10^5$, $v_3 = -0.22861578 \times 10^8$, while v_0 still keeps $v_0 = 0$ since $m_1 = m_{1H}$ still holds. This shows that we need one more perturbation on m_1 near m_{1H} such that $0 < v_0 \ll -v_1$. Since $\frac{\partial\alpha}{\partial m_1}(m_{1H}) < 0$, we take perturbation on m_1 such that $m_1 = m_{1H} + \mu$, where $\mu < 0$. Thus, finally we choose $\mu = -0.01$ to obtain $v_0 = \frac{\partial\alpha}{\partial m_1}(m_{1H})\,\mu = 0.68961642 \times 10^{-5}$, and the set of parameter values:

$$m_1 = 66.325506,\ m_2 = 0.15,\ m_3 = 0.634385,\ m_4 = 2.033215,\ m_5 = 1.165224, \tag{31}$$

which are reasonable values, compared to that given in (23). Under the above parameter values, we let the normal form equation $\dot{r}$ equal zero, yielding the polynomial equation, $v_0 + v_1 r^2 + v_2 r^4 + v_3 r^6 = 0$, which in turn results in the solutions for the amplitudes of the three limit cycles: $r_1 = 0.001927$, $r_2 = 0.011615$, $r_3 = 0.024543$. From the signs of the focus values, we know that the inner and outer limit cycles are stable since $v_1 < 0$ and $v_3 < 0$, while the one between these two limit cycles is unstable, and the equilibrium point E_1 is an unstable focus. Note that all the three limit cycles are located on an invariant manifold passing through the unstable focus E_1.

Note that under the perturbed parameter values, v_3 is in the order of 10^8. We need to check if the highest-order term in the normal form equation, $v_3 r^6$, gives a small enough value. Indeed, $v_3 r_3^6 \approx -0.004996$, shows reasonable for small-amplitude limit cycles. Further, we should point out that these limit cycles expressed in the variables X, Y and Z seem small, but they are actually in the order of $0.35 \times 10^3 \sim 0.7 \times 10^4$ when transformed back to the original variables R_n, R_d and E via (21), which are indeed comparable to solutions as shown in Fig. 4(c). The simulation result for the three limit cycles obtained from the original 3-dimensional system (20) is given in next subsection.

3.2. Simulation for three limit cycles

This subsection presents a simulation for the three limit cycles. We take the parameter values given in (31), and then use the original 3-dimensional system (20) to perform the simulation. The scaled parameters m_i, $i = 1, 2, \ldots, 5$ are transformed back to the original parameters as

$$\lambda_E = 1164.104,\quad b_3 = 0.2661,\quad \mu_n = 0.044913,\quad \mu_d = 0.295680,\quad \alpha = 0.00036633.$$

The equilibrium representing autoimmune disorder is given by

$$E_1:\quad (R_n, R_d, E) = (68224.45, 46147.49, 11718.53).$$

The simulated two trajectories are shown in Fig. 5. Fig. 5(a) depicts a 3-dimensional phase portrait in the $R_n - R_d - E$ space, and Fig. 5(b) shows the projection of the phase portrait on the $R_n - R_d$ plane, with the two initial points:

$$(R_n,\ R_d,\ E) = (68224.0,\ 46147.0,\ 12000.0),\quad (72620.0,\ 47512.0,\ 11300.0). \tag{32}$$

The first initial point is close to the equilibrium point E_1. The trajectory starting from this point converges to the smaller stable limit cycle, while the trajectory starting from the second initial point converges to the larger stable limit cycle. The unstable limit cycle is between the two stable limit cycles, restricted on an invariant manifold (which is not shown in this figure). It can be seen from this figure that the three limit cycles are located on a quite 'flat' invariant manifold (very close to a plane) whose local approximation is the center manifold associated with the Hopf bifurcation. All trajectories converge to this invariant manifold and finally either converge to the smaller limit cycle or the large limit cycle. This mathematical finding implies that the autoimmune disorder symptoms can stay in a stable chronic state with small oscillation under little outside stimuli, while this balance can be broken with intense outside perturbations such as stress, wounds, exposing

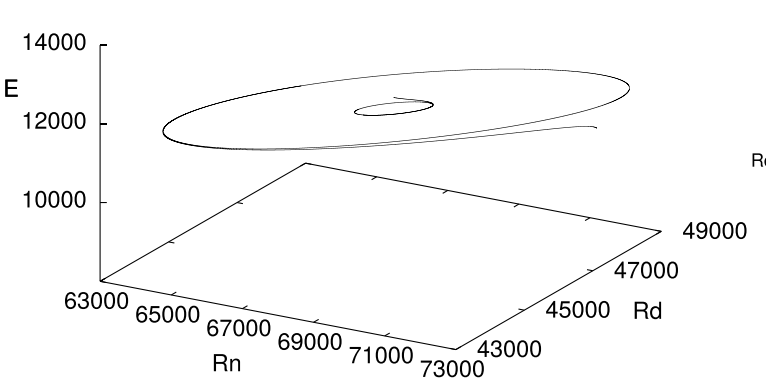

(a) 3-dimensional Phase Portrait

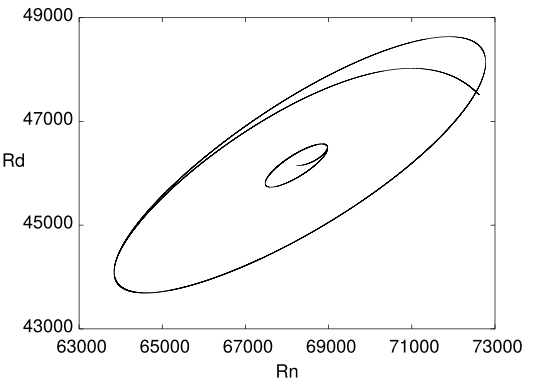

(b) 2-dimensional Phase Portrait

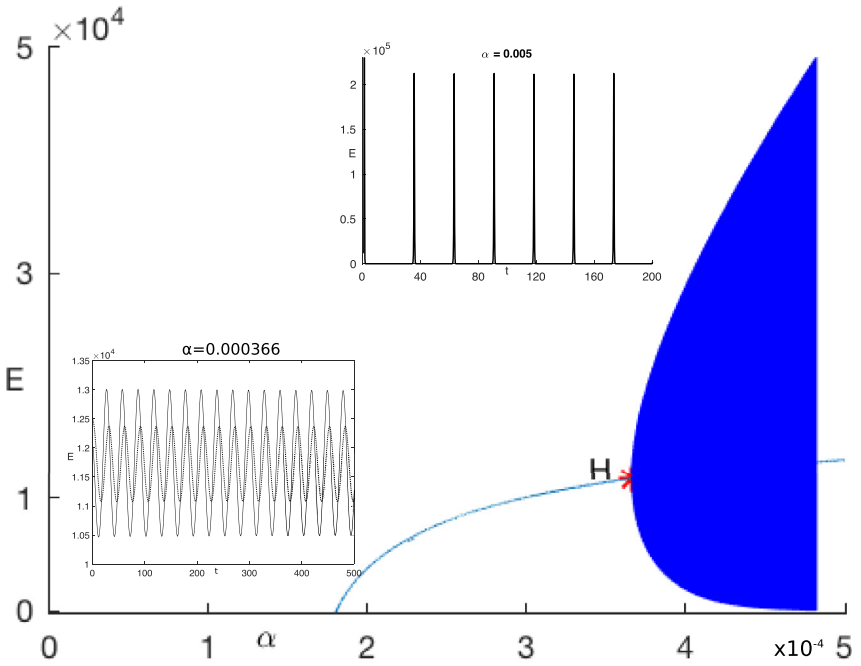

(c) Bifurcation Diagram

Fig. 5. Simulated two trajectories of the 3-dimensional model (20) for $\lambda_E = 1164.104$, $b_3 = 0.2661$, $\mu_n = 0.044913$, $\mu_d = 0.295680$, $\alpha = 0.00036633$ (and other parameter values are taken from Table 1), with one converging to the larger stable limit cycle and the other to the smaller limit cycle (the unstable limit cycle between the two stable limit cycles is not shown in the figure): (a) a 3-dimensional phase portrait in the $R_n - R_d - E$ space; and (b) a projection of 3-dimensional phase portrait on the $R_n - R_d$ plane. (c) Bifurcation diagram with the amplitude of the periodic solution from the supercritical Hopf bifurcation. One insert shows two stable limit cycles near the Hopf critical point, indicating that the effector T cell population may oscillate either along the larger limit cycle or the smaller limit cycle, depending upon initial conditions, leading to multiphase autoimmune. The other insert ($\alpha = 0.005$) denotes an special limit cycle far away from the Hopf critical point, leading to the recurrent autoimmune condition.

to sunlights, etc., which may dramatically exaggerate the autoimmune symptoms. A bifurcation diagram of the non-trivial equilibrium E_1 is plotted in Fig. 5(c), showing that a supercritical Hopf bifurcation occurs at

$$(R_n, R_d, E, \alpha) = (68226.1569, 46148.6451, 11718.6158, 0.0004).$$

The corresponding first Lyapunov coefficient from MatCont output is -9.2949×10^{-5}. Two time-history inserts are given in Fig. 4, one shows two stable periodic solutions generated from the two initial conditions in (32), and the shows the recurrent auto-reactive effector T cells.

The existence of three limit cycles shows an interesting multiphase course phenomenon in multiple sclerosis [4]. In contrast to the classical bistable states with two stable equilibria, the co-existence of three limit cycles leads to a bistable phenomenon, containing two stable and one unstable periodic solutions and two unstable equilibria (E_0 and E_1). Therefore,

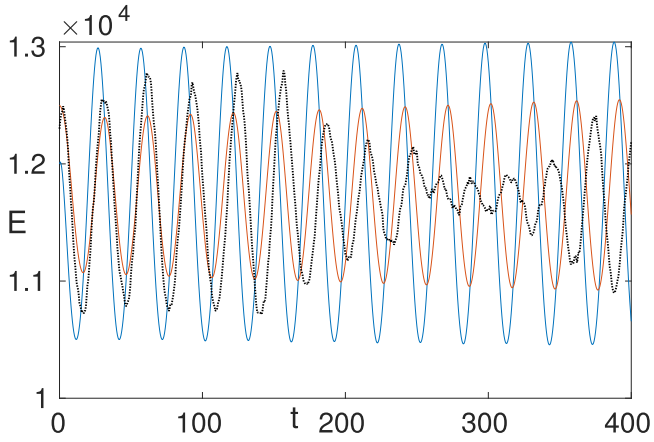

Fig. 6. Simulated Teff population time history of the 3-dimensional model (20), with the same parameter values as used in Fig. 5 (a) and (b). The red and blue curves denote two coexisting stable periodic solutions, generated using the two initial conditions given in (32). The black curve is the simulation of the trajectory when white noise (5e-3 normrnd(0, 0.5, 3) in Matlab code) is added, which travels between the red and blue stable periodic solutions. (For interpretation of the references to colour in this figure legend, the reader is referred to the web version of this article.)

depending upon the initial conditions, a trajectory eventually converges either to the smaller stable limit cycle or the larger stable limit cycle. Biologically, this phenomenon indicates that a patient could experience a more complex situation and need a careful diagnosis.

4. Conclusion and discussion

A tug of war between auto-reactive effector T cells (Teff) and regulatory T cells (Treg) can result in broad immune responses, from immune tolerance to chronic, progressive, and recurrent autoimmune disorders. The understanding of the balance between tolerance and autoimmunity is difficult. Fortunately, mathematical modeling helps to bridge the complex Teff-Treg interactions to nonlinear dynamical systems. The complex and diverse autoimmune symptoms can then be analyzed through rigorous mathematical analyses. The analytical results may provide new autoimmune-disorder causing mechanisms. In this paper, we successfully capture the multiphase lesion grade in multiple sclerosis by studying the coexistence of multiple stable cycles in a simple 3-dimensional Teff-Treg model. The multiple autoimmune-disorder oscillating stages may potentially cause the multiphase symptom.

The Teff-Treg interaction model is derived from an established 5-dimensional autoimmune disease model [32] which was used to consider the dynamics among the pAPC cells, two Treg subpopulations, Teffs, and the particular self-antigen of interest. In Section 2, we reduce the 5-dimensional model (1) to a 4-dimensional model (10) through an iterative method based on geometric singular perturbation theory, and further to a 3-dimensional model (16) according to the proportional relation between the pAPCs and Teffs. The two steps in the model reduction keep the intrinsic dynamical behaviors of the original 5-dimensional model, such as immune tolerance, chronic and relapse-remitting autoimmune disorders. Furthermore, the reduced 3-dimensional Teff-Treg model has the advantage to reveal more underlying dynamics, with the limited computational capacity. For bifurcation analysis, we choose f, the proportion of antigen molecules up-taken to lead mature pAPC, as bifurcation parameter for the 5-dimensional model. It follows that f is a factor of α in the reduced 4-dimensional and 3-dimensional models. Both f and α measure the pAPC maturation rate. The bifurcation diagrams in Fig. 4 show stable positive Teff levels at $0 < f < 5.0067 \times 10^{-4}$ in (a), $0 < \alpha < 5 \times 10^{-4}$ in (b) and $0 < \alpha = 5.66 \times 10^{-4}$ in (c), which show the bifurcation parameter values between the transcritical (BP) and Hopf (H) bifurcation points. This stable positive activated Teff level could potentially maintain the positive stable lesion grade in the chronic multiple sclerosis, as shown in Fig. 2 (a). For all three models (1), (10), and (16), Hopf bifurcations occur with the growth of pAPC maturation rates, leading to a regular oscillations for Teff population. It implies that the activation of both Teff and Treg are normally regulated with the growth of pAPC maturation rate, and the interaction between the Teff and Treg cells generates regular periodic solutions. Further increasing the pAPC maturation rate in all three models (1), (10), and (16) show recurrent Teff oscillation between the high level spikes and the low level flat bottom (see Fig. 3). It implies that the immune system with a high activation rate of pAPCs in the response to self-antigen can exaggerate the activation of both Teff and Treg. Their interaction is a tug of war, which can only suppress Teff at a low level for a period of time. Teff level can escape the suppression from time to time and shoot up to an extremely high level, which could cause irreversible damage. This explains the flat high level lesion grade in relapse-remitting multiple sclerosis data, as shown in Fig. 2(c).

To further explain the cause of the multiphase symptom in multiple sclerosis, we focus on the multiple stable coexisting periodic solutions, which can be generated from a Hopf bifurcation. Due to the heavy symbolic computation involved in analyzing the co-existing multiple limit cycles, we have used the 3-dimensional model (20) to consider only the Treg down-regulation on Teff, and rescale it to a dimensionless 3-dimensional model (22) with fewer parameters. Center mani-

fold theory and normal form theory are applied to reduce the order and parameter number to yield the normal form in the polar coordinates (19) near a Hopf bifurcation. The codimension of the generalized Hopf bifurcation can be used to determine the maximal number of small-amplitude limit cycles bifurcating in system (19) around the origin. We prove that the codimension of the generalized Hopf bifurcation is three and then use the sufficient conditions given in Theorem 3.1 to show that three limit cycles can occur (two stable ones sandwich an unstable one), enclosing a unstable equilibrium solution. The amplitudes of coexisting limit cycles from the dimensionless 3-dimensional model (19) are small, but their corresponding amplitudes in the non-scaled 3-dimensional model (20) are not, as shown in Figs. 5(a) and (b). The diverse amplitudes of the lesion grade oscillations in Fig. 2(b) may potentially be a result of a noise-driven Teff population level traveling between the coexisting stable periodic solutions, see Fig. 6. The parameter range for the existence of the coexisting three limit cycles is between two saddle-node bifurcations of periodic orbits, where two limit cycles merge and disappear. That is $\alpha \in (\alpha_{p1}, \alpha_{p2})$, where $\alpha_{p1} = 5.663989 \times 10^{-4}$ and $\alpha_{p2} = 5.663994 \times 10^{-4}$. Recalling the expression of the parameter combination $\alpha = \frac{f\tilde{\nu}\gamma}{\tilde{\nu}+\mu_G}$ in Eq. (10), we conclude that three coexisting limit cycles exist if the parameter combination of the pAPC maturation probability f and engulfing rate $\tilde{\nu}$, self-antigen release and decay rates γ and μ_G satisfies $\frac{f\tilde{\nu}\gamma}{\tilde{\nu}+\mu_G} \in (\alpha_{p1}, \alpha_{p2})$, but the region in the original parameter space is not small.

In the reduction (from the 5-dimensional system to the 4-dimensional system), the iterative method based on the geometric singular perturbation theory (GSPT) and the quasi-steady-state assumption (QSSA) method work equally well in terms of the qualitative preservation of the relapse-remitting behaviors. The iterative method gives an asymptotic expansion formula for the slow invariant manifold, which is more accurate in approximation but it involves more complicated computation in comparison with the QSSA method. In terms of the iterative method, the QSSA method is an approximation of the slow invariant manifold in the zero-order asymptotic expansions. Therefore, the parameter values for the desired model behaviors are changed between the original model and the reduced models. This discrepancy can be avoided by properly choosing parameter values as shown in Section 2. We mainly focus on the parameters in the algebraic equations of the reduced systems for their value modification, such as in the reduced 4-dimensional system. Quantitatively, the modified parameter ranges, which yield consistent behaviors during model reduction, give a guide for data fitting.

Moreover, dimensionless is a good method to reduce the computation effort. But the new dimensionless parameters are algebraic combinations of the original ones, thus hardly reflect the influence of the original parameter values on the model dynamics. We purposely keep the original parameter values in our analysis as much as possible. The parameter rescaling in (21) and (22) are reversible. This allows us to transfer the parameter values found in model (22) back to the 3-dimensional model (20) with the state variables representing Teff and Treg populations, and then guilds us for the numerical simulation on the 3-dimensional model (20), as shown in Fig. 5.

The analysis and results given in this paper also indicate that the compromise between simplicity and accuracy leads to the simplest model preserving the intrinsic dynamics and revealing the underlying mechanisms. In particular, bi-stability generated from bifurcation of three limit cycles is found from the 3-dimensional autoimmune disease model. This new and interesting bistable phenomenon only involves two stable periodic solutions (limit cycles) without any stable equilibria. The rich dynamical behaviors revealed from the 3-dimensional model may explain the observation from the clinical data in multiple sclerosis [4], which shows chronic, relapsing-remitting, and multiphase courses as depicted in Fig. 2, where the parameter data are taken from [4]. This shows that our approach presented in this paper is not only theoretically significant, but also very useful in predicting dynamical behaviors in real systems. Biologically, complex autoimmune disease patterns are demonstrated by a simple Teff-Treg interaction model, showing the important role of the Treg in T-cell-mediated autoimmunity. The Teff-Treg competition for cytokine IL-2 will be investigated in our future research.

Declaration of Competing Interest

The authors declare that they have no known competing financial interests or personal relationships that could have appeared to influence the work reported in this paper.

CRediT authorship contribution statement

Wenjing Zhang: Conceptualization, Methodology, Software, Validation, Formal analysis, Writing - original draft, Writing - review & editing. **Pei Yu:** Conceptualization, Methodology, Software, Validation, Formal analysis, Writing - original draft, Writing - review & editing.

Acknowledgment

W. Zhang was supported by Texas Tech University New Faculty Startup Funds. P. Yu was supported by the Natural Sciences and Engineering Research Council of Canada (No. R2686A02). The authors thank the two reviewers for their time and for providing very useful and detailed constructive comments and suggestions.

Appendix A.

The paper [32] shows that all solutions of the three systems (1), (10) and (16) are non-negative, if the initial conditions are taken non-negative, and moreover they are bounded. Thus, we omit this part of proving the well-posedness of the three systems, and start from determining the equilibrium solutions of these systems. Then, based on the stability of the equilibrium solutions we present a bifurcation analysis.

A1. Equilibrium solutions

It is easy to show that all the three models have two equilibrium solutions, one of them is a trivial solution (immune tolerance) E_0 at the origin, and the other is the non-trivial solution (autoimmune disorder) $\mathrm{E}_1 = (A_1, R_{n1}, R_{d1}, E_1)$, where $R_{d1} = \frac{c\xi}{\mu_d} R_{n1}$ for all three models; $G_1 = \frac{\gamma}{\tilde{\nu}+\mu_G} E_1$ for the 5-dimensional model; while

$$\begin{aligned} E_1 &= \frac{(\tilde{\nu}+\mu_G)\left[\sigma_1(\mu_d + dc\xi)R_{n1} + (b_1+\mu_A)\mu_d\right]}{f\tilde{\nu}\gamma\mu_d} A_1, \\ R_{n1} &= \frac{\mu_d\left[\pi_3(\tilde{\nu}+\mu_G)(b_1+\mu_A)A_1 + f\tilde{\nu}\beta\gamma\right]}{f\tilde{\nu}\gamma\mu_d(\mu_n+\xi) - \pi_3(\tilde{\nu}+\mu_G)\sigma_1(\mu_d+cd\xi)A_1^2} A_1, \end{aligned} \tag{33}$$

for the 5-dimensional and 4-dimensional models, provided that $\frac{f\tilde{\nu}\gamma}{\tilde{\nu}+\mu_G}$ is replaced by α for the 4-dimensional model. For the 3-dimensional model (16), the solutions for E_1 and R_{n1} are determined from two quadratic polynomials in E and R_n, which are omitted here for brevity.

A2. Stability of equilibrium E_0

To find the stability of the equilibrium solutions E_0 and E_1, we evaluate the Jacobian matrix of the linearized system at these equilibrium solutions to obtain characteristic polynomials and then use the Routh-Hurwitz criterion [14] to determine their stability. The characteristic polynomial for E_0 is given by $P_0(L) = (L+\mu_n+\xi)(L+\mu_d)\hat{P}_0(L)$, where

$$\hat{P}_0(L) = \begin{cases} L + \frac{(b_1+\mu_A)(b_3+\mu_E)-\alpha\lambda_E}{b_1+\mu_A}, & \text{for 3-dimensional model,} \\ L^2 + (b_1+\mu_A+b_3+\mu_E)L & \\ \quad + (b_1+\mu_A)(b_3+\mu_E) - \alpha\lambda_E, & \text{for 4-dimensional model,} \\ L^3 + \left[b_1+\mu_A+b_3+\mu_E+\tilde{\nu}+\mu_G\right]L^2 & \\ \quad + \left[(b_1+\mu_A+b_3+\mu_E)(\tilde{\nu}+\mu_G)\right. & \\ \qquad \left. + (b_1+\mu_A)(b_3+\mu_E)\right]L & \\ \quad + (\tilde{\nu}+\mu_G)\left[(b_1+\mu_A)(b_3+\mu_E) - \frac{f\tilde{\nu}\gamma}{\tilde{\nu}+\mu_G}\lambda_E\right], & \text{for 5-dimensional model.} \end{cases} \tag{34}$$

Noticing $\alpha = \frac{f\tilde{\nu}\gamma}{\tilde{\nu}+\mu_G}$, we can see that the trivial equilibrium of all the three models are stable (unstable) if $(b_1+\mu_A)(b_3+\mu_E) - \alpha\lambda_E > 0$ (< 0). A static bifurcation occurs at the critical point determined by $(b_1+\mu_A)(b_3+\mu_E) - \alpha\lambda_E = 0$. Further, it can be shown that the non-trivial equilibrium E_1 exists for $(b_1+\mu_A)(b_3+\mu_E) - \alpha\lambda_E \le 0$.

A3. Stability of equilibrium E_1

Next, we consider the stability of the non-trivial equilibrium E_1. Evaluating the Jacobian at E_1 yields the characteristic polynomial,

$$P_1(L) = \begin{cases} L^3 + a_{31}L^2 + a_{32}L + a_{33}, & \text{for 3-dimensional model,} \\ L^4 + a_{41}L^3 + a_{42}L^2 + a_{43}L + a_{44}, & \text{for 4-dimensional model,} \\ L^5 + a_{51}L^4 + a_{52}L^3 + a_{53}L^2 + a_{54}L + a_{55}, & \text{for 5-dimensional model,} \end{cases} \tag{35}$$

where

$$\begin{aligned} a_{33} &= \left[\alpha\lambda_E - (b_1+\mu_A)(b_3+\mu_E)\right]P_3, \\ a_{44} &= \left[\alpha\lambda_E - (b_1+\mu_A)(b_3+\mu_E)\right]P_4, \\ a_{55} &= \left[\frac{f\tilde{\nu}\gamma}{\tilde{\nu}+\mu_G}\lambda_E - (b_1+\mu_A)(b_3+\mu_E)\right]P_5, \quad \left(\frac{f\tilde{\nu}\gamma}{\tilde{\nu}+\mu_G} = \alpha\right), \end{aligned} \tag{36}$$

in which P_i, $(i = 3, 4, 5)$ are polynomial functions in the system parameters; and other coefficients a_{ij} are expressed in terms of the system parameters. It is seen that at $\alpha = (b_1+\mu_A)(b_3+\mu_E)/\lambda_E$, we have $a_{33} = a_{44} = a_{55} = 0$, and obtain $P_3 > 0, P_4 > 0, P_5 > 0$. This indicates that the equilibrium E_1 of the three models are stable if $\alpha\lambda_E - (b_1+\mu_A)(b_3+\mu_E) > 0$, and the condition, $\alpha\lambda_E - (b_1+\mu_A)(b_3+\mu_E) = 0$, defines a critical point. Comparing this stability condition with that for

the equilibrium E_0, we can conclude that for all the three models, the two equilibria E_0 and E_1 exchange their stability at a transcritical bifurcation point, determined by $\alpha\lambda_E - (b_1+\mu_A)(b_3+\mu_E) = 0$. (Note that E_1 does not exist for $\alpha\lambda_E - (b_1+\mu_A)(b_3+\mu_E) < 0$.)

It is easy to see from (34) that there is no Hopf bifurcation from the equilibrium E_0 for the 3-dimensional and 4-dimensional models. For the 5-dimensional model, it can be shown that another Routh-Hurwitz condition is also satisfied, i.e.,

$$\begin{aligned}\Delta_2 &= \left[b_1+\mu_A+b_3+\mu_E+\tilde{v}+\mu_G\right]\times\left[(b_1+\mu_A+b_3+\mu_E)(\tilde{v}+\mu_G)+(b_1+\mu_A)(b_3+\mu_E)\right]\\ &\quad -(\tilde{v}+\mu_G)\left[(b_1+\mu_A)(b_3+\mu_E)-\frac{f\tilde{v}\gamma}{\tilde{v}+\mu_G}\lambda_E\right]\\ &= (b_1+\mu_A+b_3+\mu_E)(b_1+\mu_A+\tilde{v}+\mu_G)\times(b_3+\mu_E+\tilde{v}+\mu_G)+f\tilde{v}\gamma\lambda_E > 0,\end{aligned}$$

which implies that the 5-dimensional model also does not have Hopf bifurcation from the trivial equilibrium E_0.

A.4. Hopf bifurcation from equilibrium E_1

To find possible Hopf bifurcations from the equilibrium E_1, we may use the criterion established in [28], which gives necessary and sufficient conditions for the existence of Hopf bifurcation in a general n-dimensional system as $\Delta_{n-1} = 0$ (and other stability conditions still hold), and thus we have the Hopf critical conditions determined by the following formulas for the three models:

$$\begin{aligned}&\Delta_2 = a_{31}a_{32} - a_{33} = 0, && \text{for 3-dimensional model,}\\ &\Delta_3 = (a_{41}a_{42} - a_{43})a_{43} - a_{44}a_{41}^2 = 0, && \text{for 4-dimensional model,}\\ &\Delta_4 = (a_{51}a_{52}-a_{53})(a_{53}a_{54}-a_{52}a_{55})(a_{51}a_{54}-a_{55})^2 = 0, && \text{for 5-dimensional model.}\end{aligned} \tag{37}$$

Note that all the formulas derived so far in this section are expressed explicitly in terms of the system parameters, and thus the formulas given in (37) are quite involved, in particular for Δ_4, since too many parameters are contained in the expressions.

Having established the above formulas, we can now give a general bifurcation picture for these models. Suppose the transcritical bifurcation point determined from (34) be as α_t or f_t, where the subscript index 't' denotes 'transcritical', and the Hopf bifurcation point determined from (37) as α_H or f_H, where the subscript index 'H' stands for 'Hopf'. Then, we have the following bifurcation scenario:

$$E_0 \text{ (Stable for } \alpha<\alpha_t) \overset{\alpha=\alpha_t}{\Longrightarrow} E_1 \text{ (Stable for } \alpha_t<\alpha<\alpha_H) \overset{\alpha=\alpha_H}{\Longrightarrow} \text{Limit Cycles,}$$

where α can be replaced by f for the 5-dimensional or 4-dimensional model.

Appendix B.

The lengthy expressions of the focus values v_2 and v_3 (which are used in Section 3.1) that we obtained using our Maple program [27] are listed below.

```
+18767669683*m2^31*m3*m5^2+34272855714*m2^30*m3^2*m5^2+17049557666*m2^2*m3^30*m5^2
+598625275*m2*m3^31*m5^2-2901588647*m2^30*m3*m5-14336099844*m2^29*m3^2*m5
+9908307577*m2^2*m3^29*m5+626708636*m2*m3^30*m5+288420*m2^30+288420*m3^30
-136131361040*m3^27*m2^3-136131361040*m3^3*m2^27-29286308376709*m3^6*m2^24
+794285534440798*m3^7*m2^23+6605799699718982*m3^8*m2^22+27043327850059666*m3^9*m2^21
+67091641973484364*m3^10*m2^20+95646143623375940*m3^11*m2^19+26676266499878385*m3^12*m2^18
-210004814586215727*m3^13*m2^17-526027239133365537*m3^14*m2^16-678272319459634404*m3^15*m2^15
-526027239133365537*m3^16*m2^14-210004814586215727*m3^17*m2^13+26676266499878385*m3^18*m2^12
+95646143623375940*m3^19*m2^11+67091641973484364*m3^20*m2^10+27043327850059666*m3^21*m2^9
+6605799699718982*m3^22*m2^8+794285534440798*m3^23*m2^7-29286308376709*m3^24*m2^6
-3067730145253*m3^4*m2^26-23906969662778*m3^5*m2^25-23906969662778*m3^25*m2^5
-3067730145253*m3^26*m2^4+1633976932*m2^2*m3^28+207835319*m2*m3^29-1855982700*m2^37*m5^7
+1443542100*m2^36*m5^6-866125260*m2^35*m5^5+393693300*m2^34*m5^4-131231100*m2^33*m5^3
+30284100*m2^32*m5^2+288420*m3^32*m5^2-4326300*m2^31*m5+576840*m3^31*m5+207835319*m2^29*m3
+1633976932*m2^28*m3^2+25712640*m2^45*m3^2*m5^17+1171364544*m2^44*m3^3*m5^17
+16485819408*m2^43*m3^4*m5^17+72525646728*m2^42*m3^5*m5^17-220661643960*m2^41*m3^6*m5^17
-31862880*m2^45*m3*m5^16-510409488*m2^44*m3^2*m5^16-11169364626*m2^43*m3^3*m5^16
-244620576369*m2^42*m3^4*m5^16-1941860313885*m2^41*m3^5*m5^16+454186139*m2^44*m3*m5^15
+7700014550*m2^43*m3^2*m5^15+36277936726*m2^42*m3^3*m5^15+1243187419122*m2^41*m3^4*m5^15):
```

Supplementary material

Supplementary material associated with this article can be found, in the online version, at doi:10.1016/j.cnsns.2020.105529.

References

[1] Alexander HK, Wahl LM. Self-tolerance and autoimmunity in a regulatory tcell model. Bull Math Biol 2011;73(1):33–71.
[2] Aron JL. Multiple attractors in the response to a vaccination program. Theor Popul Biol 1990;38(1):58–67.
[3] Baecher-Allan C, Wolf E, Hafler DA. MHC Class II expression identifies functionally distinct human regulatory t cells. The Journal of Immunology 2006;176(8):4622–31.
[4] Berard JL, Wolak K, Fournier S, David S. Characterization of relapsing–remitting and chronic forms of experimental autoimmune encephalomyelitis in c57BL/6 mice. Glia 2010;58(4):434–45.
[5] Carr J. Applications of centre manifold theory, volume 35. Springer Science & Business Media; 2012.
[6] de Mendizábal NV, Carneiro J, Solé RV, Goñi J, Bragard J, Martinez-Forero I, et al. Modeling the effector-regulatory t cell cross-regulation reveals the intrinsic character of relapses in multiple sclerosis. BMC Syst Biol 2011;5(1):114.
[7] DeFranco AL, Locksley RM, Robertson M. Immunity: the immune response in infectious and inflammatory disease. New science press; 2007.
[8] Dhooge A, Govaerts W, Kuznetsov YA, Meijer HGE, Sautois B. New features of the software matcont for bifurcation analysis of dynamical systems. Math Comput Model Dyn Syst 2008;14(2):147–75.
[9] Earn DJD, Rohani P, Bolker BM, Grenfell BT. A simple model for complex dynamical transitions in epidemics. Science 2000;287(5453):667–70.
[10] Fehérvári Z, Sakaguchi S. Control of foxp3+ CD25+ CD4+ regulatory cell activation and function by dendritic cells. Int Immunol 2004;16(12):1769–80.
[11] Goverman J. Autoimmune t cell responses in the central nervous system. Nat Rev Immunol 2009;9(6):393.
[12] Guckenheimer J, Holmes PJ. Nonlinear oscillations, dynamical systems, and bifurcations of vector fields, volume 42. Springer Science & Business Media; 2013.
[13] Han M, Yu P. Normal forms, melnikov functions and bifurcations of limit cycles, volume 181. Springer Science & Business Media; 2012.
[14] Hinrichsen D, Pritchard AJ. Mathematical systems theory i: modelling, state space analysis, stability and robustnes. Texts in Applied Mathematics, vol 48. 2nd edition. Springer; 2005.
[15] Jiang J, Yu P. Multistable phenomena involving equilibria and periodic motions in predator–prey systems. Int J Bifurcation Chaos 2017;27(03):1750043.
[16] Korobeinikov A, Shchepakina E, Sobolev V. Paradox of enrichment and system order reduction: bacteriophages dynamics as case study. Math Med Biol 2015;33(3):359–69.
[17] Kukreja A, Cost G, Marker J, Zhang C, Sun Z, Lin-Su K, et al. Multiple immuno-regulatory defects in type-1 diabetes. J Clin Invest 2002;109(1):131–40.
[18] Liu L, Aybar OO, Romanovski VG, Zhang W. Identifying weak foci and centers in the maxwell–bloch system. J Math Anal Appl 2015;430(1):549–71.
[19] Martinez-Forero I, Garcia-Munoz R, Martinez-Pasamar S, Inoges S, de Cerio AL, Palacios R, et al. IL-10 Suppressor activity and ex vivo tr1 cell function are impaired in multiple sclerosis. Eur J Immunol 2008;38(2):576–86.
[20] Mortell MP, O'Malley RE, Pokrovskii A, Sobolev V. Singular perturbations and hysteresis. SIAM; 2005.
[21] Phan GQ, Yang JC, Sherry RM, Hwu P, Topalian SL, Schwartzentruber DJ, et al. Cancer regression and autoimmunity induced by cytotoxic t lymphocyte-associated antigen 4 blockade in patients with metastatic melanoma. Proceedings of the National Academy of Sciences 2003;100(14):8372–7.
[22] Sakaguchi S, Sakaguchi N, Asano M, Itoh M, Toda M. Immunologic self-tolerance maintained by activated t cells expressing IL-2 receptor alpha-chains (CD25). breakdown of a single mechanism of self-tolerance causes various autoimmune diseases. The Journal of Immunology 1995;155(3):1151–64.
[23] Shchepakina E, Sobolev V, Mortell MP. Singular perturbations: introduction to system order reduction methods with applications, volume 2114. Springer; 2014.
[24] Strygin VV, Sobolev VA. Effect of geometric and kinetic parameters and energy dissipation on the orientation stability of satellites with double spin. Cosmic Res 1976;14(3):331–5.
[25] Nowak M, May RM. Virus dynamics: mathematical principles of immunology and virology: mathematical principles of immunology and virology. UK: Oxford University Press; 2000 Nov 23.
[26] Yamazaki S, Inaba K, Tarbell KV, Steinman RM. Dendritic cells expand antigen-specific foxp3+ CD25+ CD4+ regulatory t cells including suppressors of alloreactivity. Immunol Rev 2006;212(1):314–29.
[27] Yu P. Computation of normal forms via a perturbation technique. J Sound Vib 1998;211(1):19–38.
[28] Yu P. Closed-form conditions of bifurcation points for general differential equations. Int J Bifurcation Chaos 2005;15(4):1467–83.
[29] Yu P, Lin W. Complex dynamics in biological systems arising from multiple limit cycle bifurcation. J Biol Dyn 2016;10(1):263–85.
[30] Yu P, Zhang W, Wahl LM. Dynamical analysis and simulation of a 2-dimensional disease model with convex incidence. Commun Nonlinear Sci Numer Simul 2015.
[31] Zhang W, Wahl LM, Yu P. Conditions for transient viremia in deterministic in-host models: viral blips need no exogenous trigger. SIAM J Appl Math 2013;73(2):853–81.
[32] Zhang W, Wahl LM, Yu P. Modelling and anlysis of recurrent autoimmune disease. SIAM J Appl Math 2014;74(6):1998–2025.
[33] Zhang W, Yu P. Hopf and generalized hopf bifurcations in a recurrent autoimmune disease model. Int J Bifurcation Chaos 2016;26(05):1650079.